UNIVERSITY OF NAPLES FEDERICO II

DOCTORATE IN
MOLECULAR MEDICINE AND MEDICAL BIOTECHNOLOGY

XXXIII CYCLE

Angela Flavia Serpico

MITOTIC SPINDLE ASSEMBLY RELIES ON LOCALIZED CONTROL OF CDK1 ACTIVITY

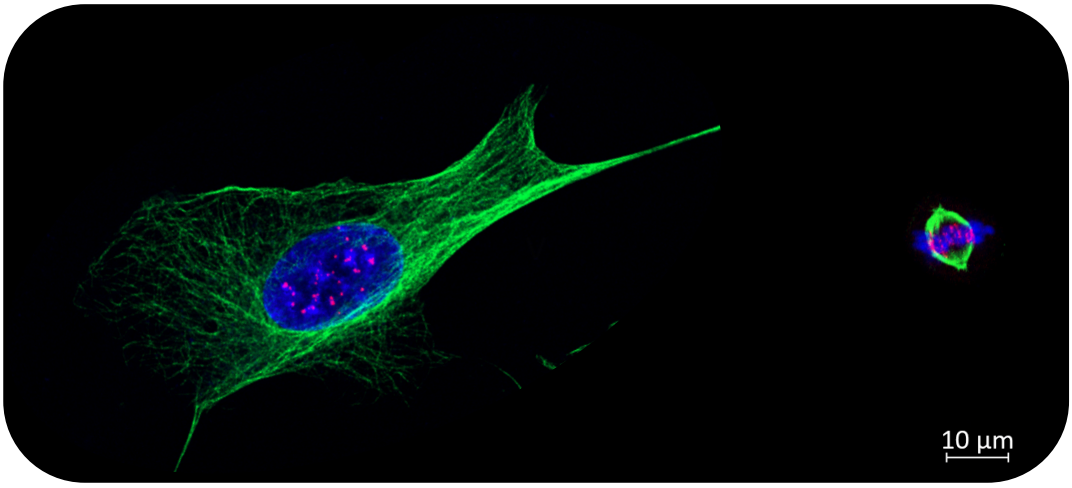

Year 2021

UNIVERSITY OF NAPLES FEDERICO II

DOCTORATE IN
MOLECULAR MEDICINE AND MEDICAL BIOTECHNOLOGY

XXXIII CYCLE

MITOTIC SPINDLE ASSEMBLY RELIES ON LOCALIZED CONTROL OF CDK1 ACTIVITY

Tutor
Ch.mo Prof. Domenico Grieco

Candidate
Angela Flavia Serpico

Year 2021

INDEX

I. LIST OF ABBREVIATIONS

I. LIST OF ABBREVIATIONS

A: alanine
APC/C: anaphase-promoting complex/cyclosome
ATP: adenosine triphosphate
CAK: cdk-activating kinase
Cdc20: cell division cycle 20 protein
Cdc25: cell division cycle 25 phosphatase
cdk1: cyclin-dependent kinase 1
Cdk1: cyclin B1/cdk1 complex
cdk1AF: mutant of cdk1 rendered non phosphorylatable at T14 and Y15
Cdks: cyclin-dependent kinases
cdk1WT: cdk1 wild type
ch-Tog: colonic and hepatic tumor overexpressed gene
CHX: cycloheximide
DTT: 1,4-Dithiothreitol
EGTA: ethyleneglycol- bis(2-aminoethyl)-N,N,N′,N′-tetraacetic Acid
F: phenylalanine
FLB: fractionation lysis buffer
GCPs: γ- tubulin complex proteins
GDP: guanosine 5'-diphosphate
GTP: guanosine 5'-triphosphate
high-RO: RO-3306 at 9 μM
HSB: high salt lysis buffer
i-Cdk1: inhibited form of Cdk1
Ibs: immunoblotting
IF: indirect immunofluorescence
Ips: immunoprecipitations
k-fiber: kinetochore fiber
KRB: kinase reaction buffer
LB: lysis buffer
low-RO: RO-3306 at 0,5 μM
M/C medium: medium supplemented with MG-132 and CHX
Map4: microtubule associated protein 4
MAPs: microtubule associated proteins
Meta cells: metaphase-arrested cells
MTB: microtubule binding domain
MTOCs: microtubule-organizing centers
MTs: microtubules

Myt1: membrane-associated tyrosine- and threonine-specific cdc2-inhibitory kinase
NuMA: nuclear mitotic apparatus protein
P fraction: pellet fraction
p-Y15-cdk1: cdk1 phosphorylated at tyrosine 15
PCM: pericentriolar material
Plk1: polo-like kinase 1
PP1: serine/threonine protein phosphatase 1
PP1α: PP1 α isoform
PP1C: PP1 catalytic subunit
PP2A: serine/threonine protein phosphatase 2A
PRB: phosphatase reaction buffer
Pro cells: prometaphase-arrested cells
S: serine
S fraction: supernatant fraction
SDS: sodium dodecyl sulfate
siRNAs: small interfering RNAs
T: threonine
tGFP-Map4-PP1-KO: turbo-GFP-Map4 defective in PP1 binding to Map4
tGFP-Map4-S787A: turbo-GFP-Map4 rendered non phosphorylatable at S787
tGFP-Map4-WT: turbo-GFP-Map4-wild type
V: valine
W: tryptophan
WB: washing buffer
Wee1: Wee1-like protein kinase
Y: tirosine
γ-TuRCs: γ-tubulin ring complexes
γ-TuSCs: γ-tubulin small complexes

II. ABSTRACT

II. ABSTRACT

During cell division, mitosis involves profound rearrangements of the cytoskeleton such that the interphase microtubular network is rapidly dismantled while highly dynamic microtubules (MTs) nucleated from centrosomes start a chromosome search and capture process to build up the mitotic spindle, the structure deputed to chromosome segregation. The wholesale MT reorganization at mitotic entry is triggered by the activation of cyclin B/cyclin-dependent kinase 1 (cdk1) complex (Cdk1). During interphase, Cdk1 is kept inactive by Wee1-like protein kinase (Wee1)- and membrane-associated tyrosine- and threonine-specific cdc2-inhibitory kinase (Myt1)-dependent inhibitory phosphorylation while, at mitosis onset, Cdk1 gets activated via dephosphorylation at these sites by cell division cycle 25 phosphatase (Cdc25) and starts positive feedback loops that ensure its full activation. Active Cdk1 drives dissolution of the long interphase MT arrays by phosphorylating and inhibiting stabilizing microtubule associated proteins (MAPs), like microtubule associated protein 4 (Map4) and colonic and hepatic tumor overexpressed gene (ch-Tog). Nevertheless, most of these MAPs are required for spindle MT growth. How mitotic spindles assemble overcoming the highly MT destabilizing environment imposed by active Cdk1 is unknown.
During this work we uncovered that a small fraction of Cdk1, exclusively localized at spindle structures, avoided Cdc25 activating action and persisted in a phosphorylated and inhibited form (i-Cdk1). Abating i-Cdk1 impaired spindle assembly while its restoration rescued normal spindle formation. We found that centrosomes and their nucleating MTs promoted i-Cdk1 formation by tightly binding Wee1 but not Cdc25. Moreover, i-Cdk1 was required to locally promote serine/threonine protein phosphatase 1 (PP1)-dependent reversal of inhibitory phosphorylation of stabilizing MAPs for spindle MT growth. Thus, these data highlight a new control element for spindle assembly relying on compartmentalized control of Cdk1 activity.

III. BACKGROUND

III. BACKGROUND

III.1 Brief synopsis of mitosis

Mitosis is the eukaryotic cell cycle phase deputed to precisely separate and segregate replicated chromosomes into two identical sets, when a mother cell duplicates in two daughter cells. To achieve this goal cells undergo profound structural rearrangements ending up with the assembly of an ad hoc cytoskeletal apparatus – the mitotic spindle - that both drives the duplicated sister chromatids to bisect and the cytoplasm to halve (McIntosh, 2016).

Mitosis (nuclear division) and cytokinesis (cell division) collectively form the M phase and occupy only a restricted fraction (1 hour) of the cell cycle (24 hours long) in a typical proliferating mammalian cell, which is mostly constituted by a longer portion known as interphase (Figure 1). During interphase cells continuously grow, metabolize nutrients, replicate DNA, duplicate proteins and organelles, and prepare for mitosis (Morgan *et al*., 2015).

The wide changes occurring during the M phase come in succession through six stages. At prophase, cytoplasmic MTs dissolve, chromosomes condense within the nucleus and outwardly short and dynamic MTs start radiating from each centrosome to form the bipolar spindle. During prometaphase, the nuclear envelope breaks down and the MTs elongating from the spindle set about searching for chromosomes. The ensuing chromosome lineup at the cellular equatorial level marks metaphase. During anaphase, chromosome spindle-bound fibers depolymerize leading sister chromatids to split off and move towards opposite poles of the spindle. At telophase, both sets of daughter chromosomes begin to decondense, lose contact with spindle MTs and become surrounded by a new nuclear envelope. Simultaneously, the cytoplasm is divided in two by cytokinesis through a contractile ring of actin and myosin

filaments, so that the two daughter cells finally form by abscission, the ultimate step of separation (Morgan *et al.*, 2015; Figure 1).

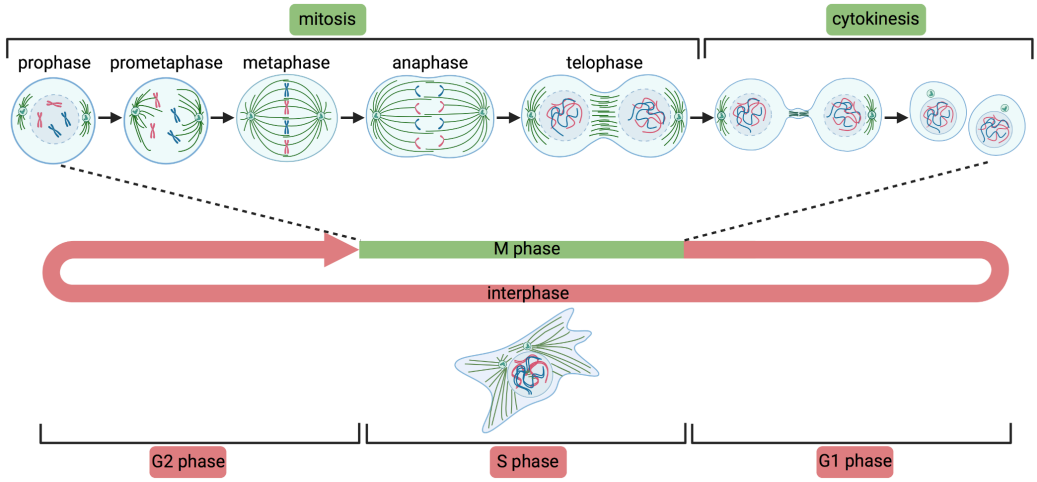

Figure 1 | Cell division cycle in eukaryotic cells. Diagram showing the phases of cell cycle. Interphase and M phase constitute the two major phases of cell cycle. Interphase consists of three stages: G1 phase, S phase, G2 phase. G phases are gap phases situated between M phase and S phase (G1 phase) and between S phase and M phase (G2 phase). S phase delimits DNA replication. M phase includes mitosis and cytokinesis. In interphase chromosomes are largely decondensed and accurately contained in the nucleus while outwardly MTs extend from the centrosome throughout the cytoplasm in a radial array. At prophase, chromosomes become highly condensed, nuclear envelope begins to breakdown, centrosomes start separating and the wide interphase MT network progressively depolymerizes. At prometaphase, nuclear membrane completely dissolves making chromosomes no more constrained in the nucleus and spindle MTs able to capture them. At metaphase, chromosomes reach congression at the spindle equator. During anaphase, chromosomes move towards the poles. During telophase chromosomes start to decondense and nuclear envelope reforms. During cytokinesis the cytoplasm is divided in two identical parts and each daughter nucleus is distributed in an individual cell.

III.2 MT structure and dynamics

Since 1963, when enhanced fixation methods allowed Slautterback, Ledbetter and Porter to certainly define MTs, our knowledge about these ubiquitous cellular structures is constantly evolving (Wells, 2005).

MTs are long hollow polymers composed of α- and β- tubulin heterodimers aligned head-to-tail, generally ≈ 25 nm wide and 1 - 100 µm long. Each fiber is composed of 13 linear protofilaments assembled laterally to form polar rods.

Indeed, the resulting polymer has a fast-growing plus end that exposes β-tubulin monomers and a slow-growing minus end that exhibits α-tubulin ones (Figure 2).

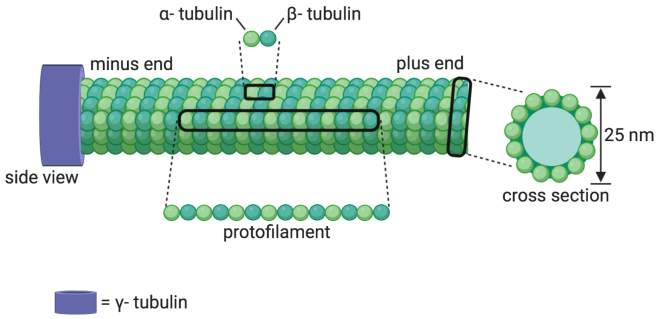

Figure 2 | MT structure. Model summarizing key components of MT structure, as indicated.

Both α and β subunits bind the nucleotide guanosine triphosphate (GTP), but only the β-tubulin hydrolyzes GTP into guanosine diphosphate (GDP) (Goodson *et al.,* 2018). MT growth results from GTP-tubulin subunits addition to their plus ends. After subunits are integrated into MT lattice, their GTP undergoes hydrolysis into GDP. GDP-tubulin is forced to be in an unfavorable conformation within MT fibers, thus promoting their shrinking (Figure 3). This special property of α- and β-tubulin, depending on which energy carrier nucleotide is bound to them, explains the rapid switch between elongation and shortening phases that MTs can undergo several times during their lifetime, known as dynamic instability (Kirschner *et al.,* 1986b; Burbank *et al.,* 2006). MT dynamics can be defined by some parameters. The growth and shrinkage rates are quantified as the frequency of incorporation and detachment of GTP-tubulin subunits at the MT plus ends, respectively. Catastrophe is the MT transition from a growing state to a shrinking state. Vice versa, rescue refers to the MT transition from a shrinking state to a growing state (Margolin *et al.,* 2012; Figure 3).

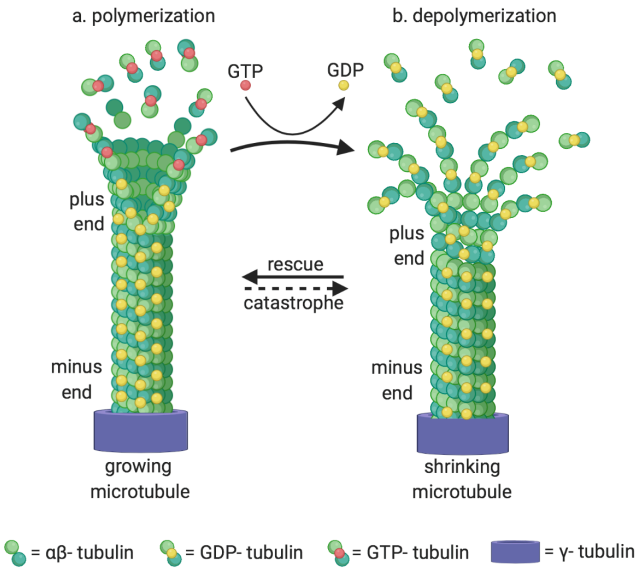

Figure 3 | MT dynamics. a, GTP-tubulin subunits addition (red) to plus ends drives MT growth. After incorporation, GTP subunits undergo hydrolysis to GDP subunits. **b**, GDP-tubulin subunits in the MT lattice are forced to assume an unfavorable conformation, thus induce MTs to shrink.

Because of their structure, MT plus ends regulate the extent of MT array, while the minus ends determine the structure of MT networks. Indeed, the MT minus ends are composed of a layer of GTP-tubulin trapped in a γ-tubulin complex cap, that protects them from polymerization and – as shown below - serves as MT nucleating site.

III.3 MT nucleation and centrosomes

α/β-tubulin heterodimers assembly is a kinetically unfavorable process, so much so that it rarely spontaneously occurs *in vivo*. A nucleating factor is required to trigger this polymerization process (Petry *et al.,* 2015). γ-tubulin, a member of the tubulin superfamily, ensures MT nucleation in eukaryotes. Indeed, it assembles with other proteins to form the γ-tubulin ring complexes (γ-TuRCs), that foster the assembly of MTs (Tovey *et al.,* 2018).

In vertebrates γ-TuRC is a multi-protein complex composed of γ-tubulin, five related γ-tubulin complex proteins (GCPs) and related factors (Zheng *et al.,* 1995; Wu *et al.,* 2017; Liu *et al.,* 2019). In detail, γ-tubulin small complexes (γ-TuSCs), containing two molecules of γ-tubulin associated with a dimer of GCP2 and GCP3 proteins, oligomerize into larger structures to form the γ-TuRCs, along with several additional factors, namely GCP4, 5, 6 (Doxsey, 2001; Remy *et al.,* 2013; Figure 4a and 4b).

γ-TuRCs surround MT minus ends by tying to their α-tubulin subunits (Akhmanova *et al.,* 2019), so that MTs protrude outward with their minus ends anchored to them and the growing plus ends moving toward the opposite direction (Figure 4c). In particular, both at interphase and mitosis, the most part of γ-TuRCs are dispersed within the pericentriolar material (PCM) of centrosomes, constituting the platforms to MT nucleation, also known as microtubule-organizing centers (MTOCs) (Vertii *et al.,* 2016; Figure 4d).

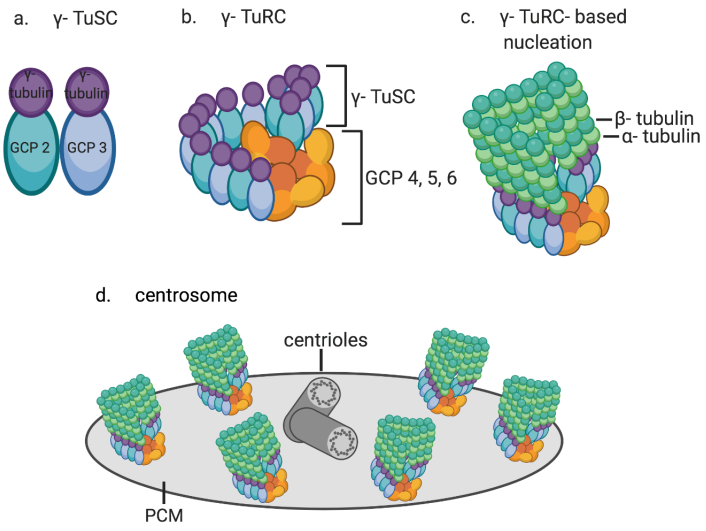

Figure 4 | γ- tubulin prior complexes. a, Two copies of γ- tubulin associate with GCP2 and GCP3 to form the γ- TuSC. **b**, Multiple γ- TuSCs assemble with GCP4, GCP5 and GCP6 and arrange into larger ring shape structures, the γ- TuRC. **c**, γ-TuRC acts as a cap-like scaffold, exposing γ-tubulin subunits to make contact with α/β-tubulin dimers. **d**, Several γ-TuRCs localize within the pericentriolar material (PCM) of centrosomes.

In interphase, the centrosome is located nearness to the cell nucleus and duplicates. In early mitosis the centrosomes separate, maturate and progressively migrate to the opposite poles of the cell to form the mitotic spindle (Petry, 2016; Vertii *et al.,* 2016; (Figure 5). During maturation, centrosomes undergo to a progressive enrichment of proteins at their PCM, so much that PCM enlarges and develops an outer expansive layer that promotes MT nucleation capacity (Fry *et al.,* 2017; Figure 5). Cdk1, Polo-like kinase 1 (Plk1) and Aurora A kinases play a key role in this process (Wang *et al.,* 2014). Nuclear mitotic apparatus protein (NuMA) is included among the most abundant proteins recruited at PCM at mitosis onset and serves as mitosis-specific MT minus end cargo adaptor (Zeng, 2000; Hueschen *et al.,* 2017).

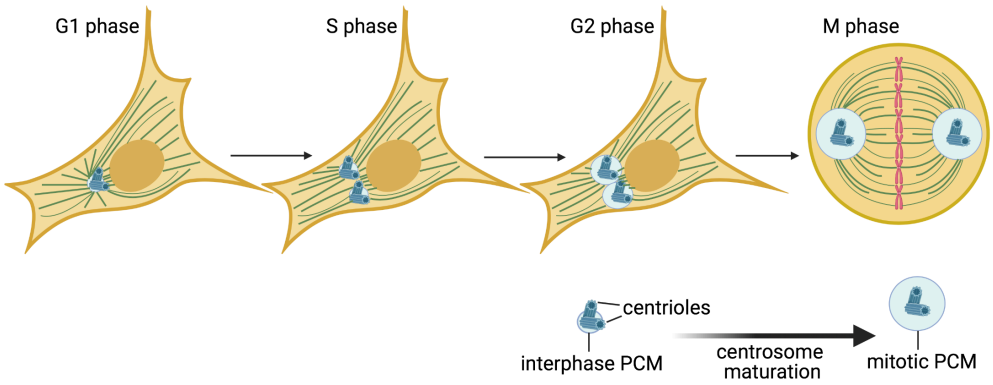

Figure 5 | Centrosome location during cell cycle. At interphase, the centrosome is next to the nucleus. During S phase, the centrosome duplicates and divides. Starting from G2 phase, the centrosomes undergo progressive maturation, which is accomplished in M phase. During M phase, the centrosomes place at the opposite poles of the cell.

The spindle apparatus positions chromosomes at the equatorial plane of the cell and drives sister chromatids to move towards the opposite poles so that each daughter cell inherits a single copy of the genome. Since Flemming's description in animal cells in 1882, the mitotic spindle is one of the most challenging systems to understand. According to early spindle models, the spindle constructing MTs individually originate from spatially defined foci, the centrosomes (Kirschner *et al.,* 1986a; Petry, 2016), and a cluster of ~20-40

MTs attach to the kinetochore of each sister chromatids (k-fibers) (DeLuca *et al.*, 2012; Figure 6a). However, more recent works, along with computational modeling, suggested that the probability of centrosome-nucleated MTs to contact all kinetochores without exceeding the short duration of mitosis is extremely low (Wollman *et al.,* 2005) and unveiled centrosome-independent MT growth during mitosis (Petry *et al.,* 2015; Meunier *et al.,* 2016; Scrofani *et al.,* 2016). Indeed, in human metaphase spindles γ-TuRCs and similar γ-tubulin-dependent nucleating centers are recruited at pole-distal regions and/or intra-spindle regions and bound to minus ends of non-centrosomal spindle MTs (Lecland *et al.,* 2014; Figure 6b). Thus, during mitotic spindle assembly, MTs nucleate not only at centrosomes but also within regions around chromosomes (Gruss *et al.*, 2002; Sampath *et al.,* 2004) and from pre-existing centrosomal MTs (branching MTs) (Goshima *et al.,* 2008; Petry *et al.,* 2011; Kamasaki *et al.,* 2013; David *et al.,* 2019; Figure 6b).

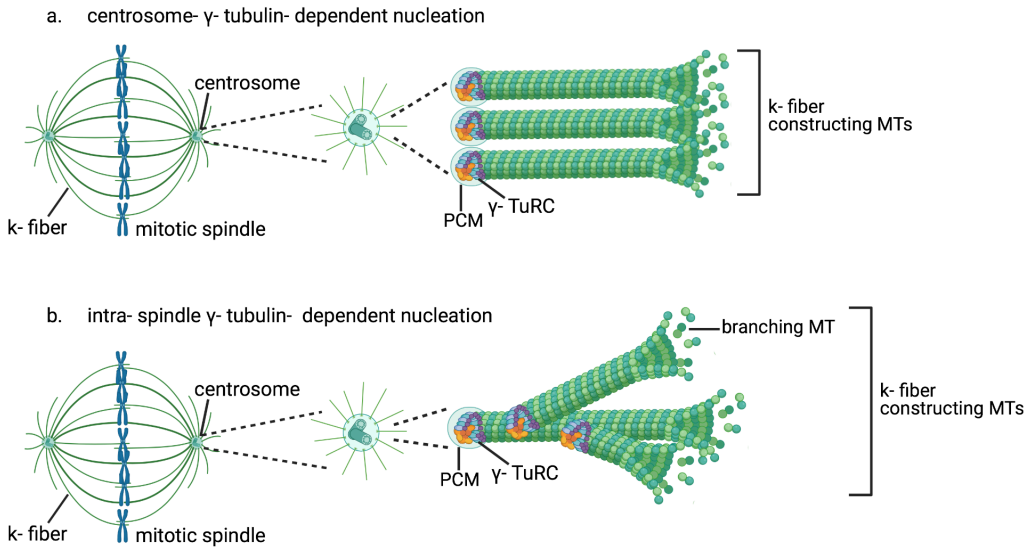

Figure 6 | Model for γ-tubulin dependent nucleation of MTs. a, Early models reported that k-fiber constructing MTs nucleate individually from centrosomes. **b**, Recent evidences suggest γ-TuRCs are recruited on pre-existing MTs by spindle-bound proteins (not shown) and drive branching MTs nucleation starting from intra-spindle poles.

III.4 Cdk1 activity regulation in and out of mitosis

Cdk1 functions as the universal inducer of G2/M phase transition and the master regulator of mitosis in eukaryotic cells (Gavet *et al.,* 2010; Kishimoto, 2015). Initial observations date back to 70s, when Masui and co-workers discovered a meiotic maturation promoting factor in frog oocytes (Masui *et al.,* 1971; Wasserman *et al.,* 1976). Later, that factor was purified from mitotic *Xenopus l.* and starfish eggs and identified as the heterodimer cyclin B-cdk1 (Labbé *et al.,* 1989; Gautier *et al.,* 1988; Lohka *et al.,* 1988a).
During G2 phase, cyclin B binds to cdk1, and the Cdk1 complex is concomitantly phosphorylated by cdk-activating kinase (CAK) at threonine 161 (T161) of cdk1, a phosphorylation required for T-loop activation (Krek *et al.,* 1992, Solomon *et al.,* 1992), and by the Wee1 kinase family members Wee1 and Myt1 that phosphorylate cdk1 at threonine (T) and tyrosine (Y) residues in the ATP binding site, phosphorylations that inhibit Cdk1 activity (O'Farrell, 2001). In human cells, Wee1 phosphorylates cdk1 at Y15 while Myt1 has a dual activity on T14 and Y15 residues (Parker *et al.,* 1992; Fattaey *et al.,* 1997; Mueller *et al.,* 1995; Liu *et al.,* 1997;). Together, Wee1 and Myt1 ensure that Cdk1 remains inactive until M phase onset when, upon DNA replication completion, the cell division cycle 25 (Cdc25) phosphatase sets off Cdk1 activation, rapidly dephosphorylating cdk1 T14 and Y15 residues (Strausfeld *et al.,* 1991; Perry *et al.,* 2007). Once activated, Cdk1 phosphorylates Wee1 and Myt1, inhibiting their activities (McGowan *et al.,* 1995; Watanabe *et al.,* 2004; Watanabe *et al.,* 2005; Nakajima *et al.,* 2004;), while it phosphorylates Cdc25 and stimulates its activity, promoting this way auto-activatory feedback loops (Kumagai *et al.,* 1992; Hoffmann *et al.,* 1993; Trunnell *et al.,* 2011). Thus, Wee1, Myt1 and Cdc25 regulate Cdk1 but they are in turn regulated by Cdk1. This interlocking system results in a double negative feedback loop (Wee1/Myt1 – Cdk1 – Wee1/Myt1) and a positive feedback loop (Cdc25C – Cdk1 – Cdcd25), that together rule Cdk1 self-

sustaining activity during mitosis until the metaphase to anaphase transition (Novak *et al.,* 1993; Thron, 1996). At this time, Cdk1 gets inactivated as a consequence of ubiquitin-dependent degradation of cyclin B by the anaphase-promoting complex/cyclosome (APC/C ^{Cdc20}) (Clute *et al.,* 1999; Castro *et al.,* 2005; Musacchio *et al.,* 2007; Figure 7).

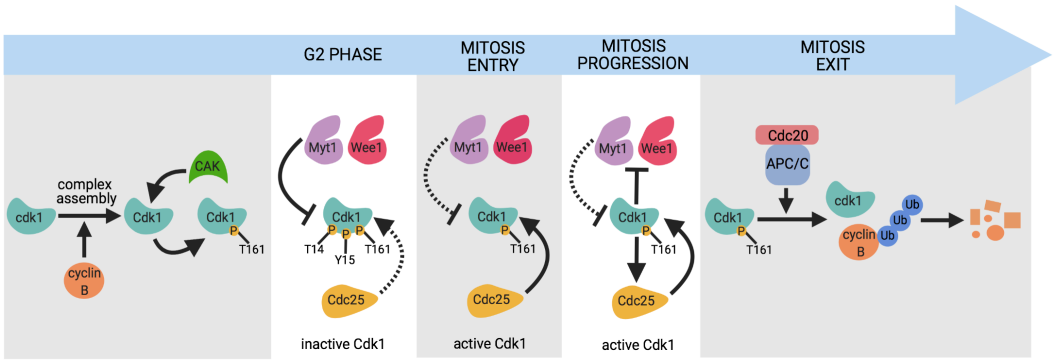

Figure 7 | Fine tunings control Cdk1 activity during mitosis. Cyclin B accumulates post S phase and associates with cdk1. Cdk1 complex activation requires CAK-dependent phosphorylation at T161 of cdk1 subunit. Because of its crucial role in cell division, Cdk1 activity is tightly regulated. Myt1 and Wee1 kinases restrain Cdk1 activity during G2 phase by inhibitory phosphorylation at T14 and Y15 of cdk1, respectively. At mitosis onset, Cdc25 phosphatase removes those inhibitory phosphates and activates Cdk1. Cdk1 itself sustains its activity throughout mitosis initiating auto-activatory feedback loops: it phosphorylates and activates Cdc25 phosphatase, while it phosphorylates and inhibits Myt1 and Wee1 kinases. Cdk1 gets inactivated as a result of APC/C^{Cdc20} – dependent degradation of cyclin B.

Importance of Cdk1 activity regulation is evident from some data in the literature. Indeed, premature Cdk1 activation, like that deriving from overexpression of a non phosphorylatable mutant of cdk1 at its inhibitory sites T14 and Y15 (cdk1AF), induces early entry into mitosis (Krek *et al.,* 1991b). Importantly, cdk1AF overexpression impairs spindle assembly (Krek *et al.,* 1991b) (Figure 8). These mitotic defects were explained as a result of an override of the normal G2/M checkpoint mechanism (Krek *et al.,* 1991b).

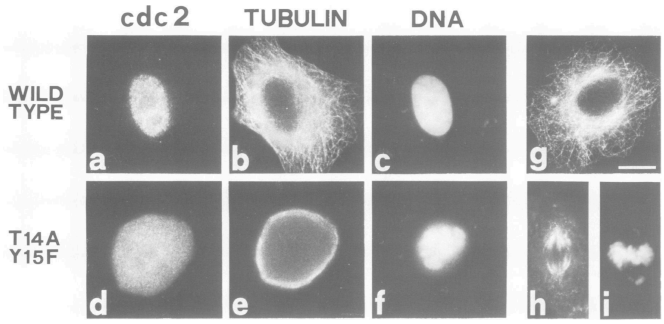

Figure 8 | Cdk1AF overexpression impairs spindle assembly. HeLa cells were transfected with either wild type chicken $p34^{cdc2}$ - another name for cdk1 kinase – (a - c) or the double non phosphorylatable mutant T14AY15F $p34^{cdc2}$ (cdk1AF) (d - f). 30 hours post transfection cells were processed for indirect immunofluorescence microscopy using anti-$p34^{cdc2}$ antibody (a, d), anti-tubulin antibody (b, e) and the DNA stain Hoechst dye 33258 (c, f). (g) shows tubulin staining of an untransfected interphase HeLa cell. (h) and (i) illustrate an untransfected metaphase HeLa cells probed for tubulin (h) and DNA staining (i). Bar in (g): 15 μm (From Krek *et al.,* 1991b).

Moreover, later studies have refined knowledge on Cdk1 activity in mitosis, reporting that phosphorylated Cdk1 at its inhibitory sites is present both in meiotic and mitotic extracts form *Xenopus* and mouse eggs (D'Angiolella *et al.,* 2007; Oh *et al.,* 2011; Figure 9).

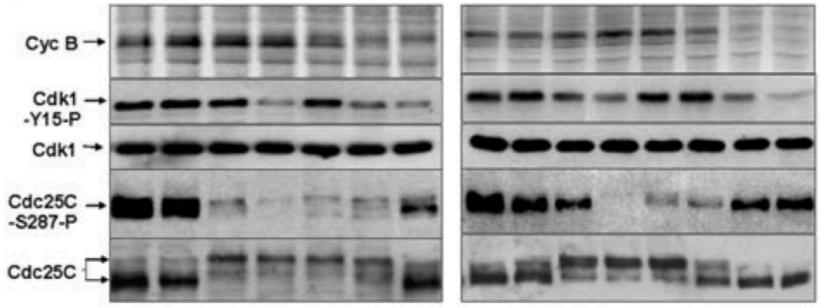

Figure 9 | Cdk1 activity in cycling *Xenopus l.* egg extracts. Cyclin B (Cyc B) autoradiographs and phospho-tyr15-cdk1 (Cdk1-Y15-P), cdk1 (Cdk1), phospho-ser-287-Cdc25C (Cdc25C-S287-P), cdc25C (Cdc25C) immunoblots from samples of two independent cycling *Xenopus l.* egg extracts, incubated in the presence of [^{35}S]methionine, taken at 2 min intervals. Cdk1 undergoes Y15 phosphorylation twice during the mitosis-to-interphase transition. An initial Cdk1-Y15-P decrease corresponds to cyclin B/cdk1 activation at mitosis onset. Then, Cdk1-Y15-P signal transiently increases just around the time of cyclin B degradation initiation and decreases again when cyclin B degradation almost accomplished (Adapted from D'Angiolella *et al.,* 2007).

III.5 Cdk1 effects on MT remodeling

Cdk1 exerts extensive protein phosphorylation, that ensure counteracting phosphatase repression until metaphase to anaphase transition, when their activity is restored in order to support mitosis completion (Wurzenberger *et al.,* 2011; Hégarat *et al.,* 2016; Figure 10).

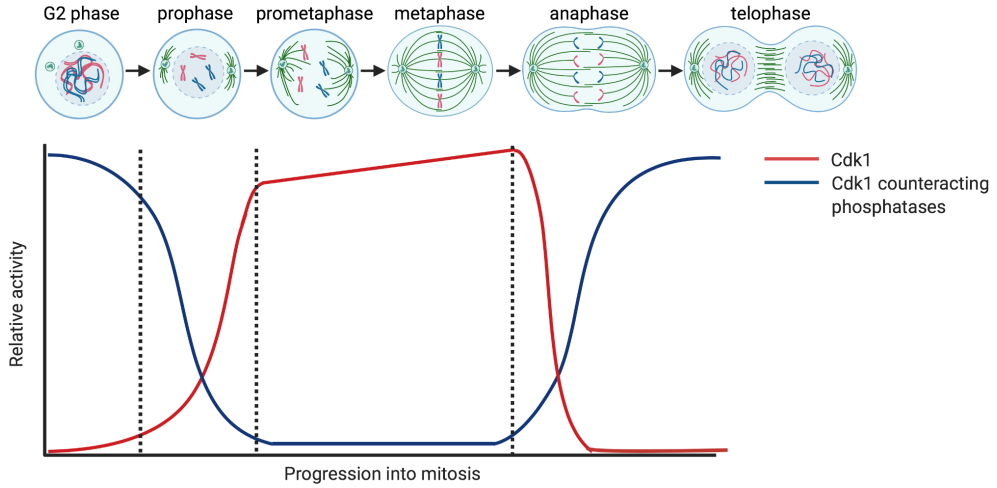

Figure 10 | Cdk1 opposes major mitotic phosphatases. Cdk1 activity increases as the cells enter mitosis (red line). Major mitotic phosphatases, including PP1 and PP2A, counteract Cdk1 activity and their activity decreases until metaphase to anaphase transition (blue line). At this time, in consequence of Cdk1 activity decline because of cyclin B degradation, phosphatases regain complete activity (blue line).

Cdk1 directly and indirectly restrains the major mitotic phosphatases, like serine/threonine protein phosphatase 1 (PP1) and serine/threonine protein phosphatase 2A (PP2A; Qian *et al.,* 2013). Indeed, as cells enter mitosis Cdk1 inhibits PP1 phosphatase function by phosphorylating their catalytic subunit (PP1C), in particular the α isoform (PP1α) at threonine 320 (p-T-320-PP1α) and the other PP1 isoforms in analogous sites (Dohadwala *et al.,* 1994; Kwon *et al.,* 1997). At later stages of mitosis, PP1 auto-dephosphorylates and activates, as a consequence of Cdk1 inactivation (Wu *et al.,* 2009).

The phosphorylation wave triggered by Cdk1 at early M phase also acts to timely rearrange cell architecture and make it suitable for mitosis (Nigg, 1993).

The cytoplasmic interphase MT complex dissolution makes the cytoplasm an environment suitable for mitotic spindle MT growth and for safe chromosome segregation (Mchedlishvili *et al.,* 2018). Early evidence in *Xenopus l.* egg extracts show that Cdk1 activation increases the MT catastrophe rate (Belmont *et al.,* 1990) and drives the interphase MT networks to a complete destabilization (Lamb *et al.,* 1990; Verde *et al.,* 1990; Lieuvin *et al.,* 1994; Ubersax *et al.,* 2003; Figure 11).

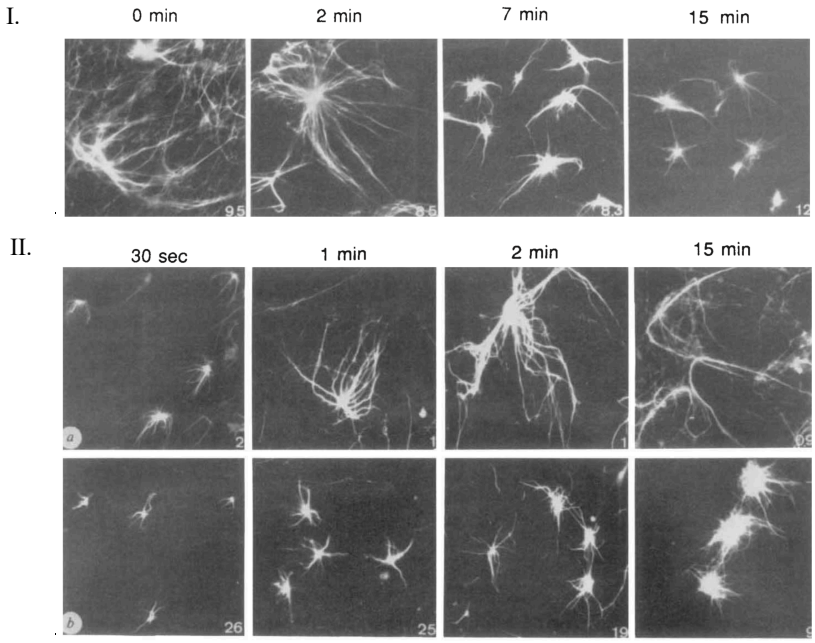

Figure 11 | Effect of Cdk1 on MT length and elongation rate in interphase egg extracts. **I**, Interphasic asters were obtained from centrosomes pre-incubation at room temperature for 10 min in an interphase *Xenopus* egg extract. Cdk1 kinase was then added and samples were fixed for immunofluorescence at the indicated time. Two min after Cdk1 addition, free MTs disappeared. Then, centrosome-nucleated MTs started to shrink (7 min) and continued to shrink until reaching a 7 µm stable length (15 min). **II**, Interphasic asters were obtained from centrosome pre-incubation in an interphase Xenopus egg at room temperature for 15 min without (a) and with (b) Cdk1. The elongation rate and the MT length in the Cdk1-treated extract dropped at 1 min compared to the untreated extract. (Adapted from *Verde et al.,* 1990).

In particular, Cdk1 directly antagonizes some stabilizing MAPs, like Map4 and ch-Tog (Ookata *et al.,* 1997; Vasquez *et al.,* 1999; Charrasse *et al.,* 2000), inducing them to dissociates from the MT lattice (Drewes *et al.,* 1998) or reducing their ability to stabilize MTs (Ookata *et al.,* 1995).

III.6 MT stabilizing MAPs

Bare MTs are unsteady structures able to quickly adapt to the cell needs. To balance their intrinsic instability, MTs are constantly assisted in their functions by a variety of specialized interacting proteins (Goodson *et al.,* 2018). MAPs are directly bound to tubulin subunits, probably by electrostatic interaction between the positive charge they are endowed with and the negatively charged C-terminal end of tubulin (Kavallaris *et al.,* 2008).

MAPs, whose basic domains and features are well conserved among different cell types, can be functionally categorized as MT stabilizers and destabilizers. Stabilizing MAPs promote MT polymerization and/or reduce depolymerization, generally by localizing at the plus end tips of MTs and stabilizing their growing conformation, or by placing along the MT lattice and acting as cross-linkers among neighboring fibers. Ch-Tog and Map4 belong to these categories, respectively (Nguyen *et al.,* 1997; Charrasse *et al.,* 1998; Ohkura *et al.,* 2001). On the contrary, destabilizing MAPs induce MTs to depolymerize by binding free tubulin or MT growing tips, suppressing subunit addition (Kavallaris *et al.,* 2008; Goodson *et al.,* 2018).

MAPs exert their function throughout the cell cycle, by both tightening up the interphase cytoskeleton and building up the mitotic spindle.

Many types of MAPs share a common mechanism of regulation for MT interaction, i. e. phosphorylation at their C-terminal microtubule binding domain (MTB; West *et al*., 1991). Generally, stabilizing MAPs in their phosphorylated forms lose the ability to bind MTs, resulting in MT instability increase (Figure 12).

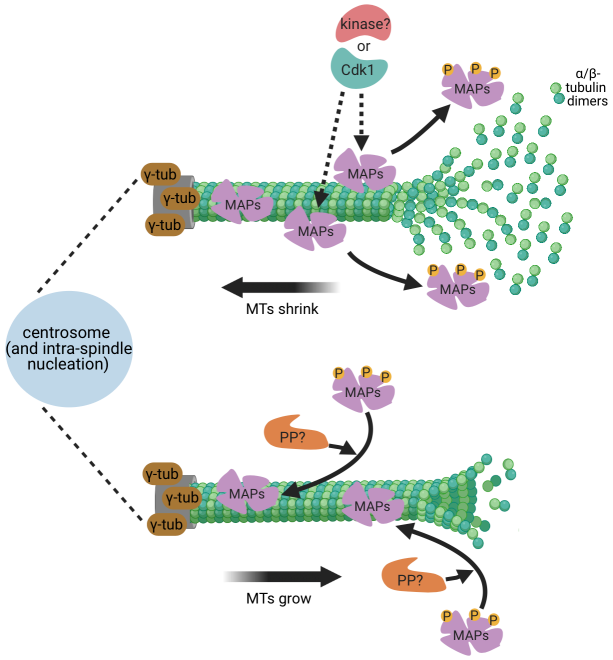

Figure 12 | Schematic representation of MAP interaction with MTs. Phosphorylation at their MBD regulates stabilizing MAP interaction with MTs. Phosphorylated MAPs dissociate from MTs causing shrinkage increase. Removal of MAP phosphorylation allows them to promote MT growth and stabilization.

Among stabilizing MAPs, Map4 and ch-Tog are expressed almost ubiquitously in vertebrate cells and are the most characterized both structurally and functionally.

Map4 is the major MAP found in proliferating non-neuronal cells. It associates with interphase MTs and mitotic spindle fibers, promotes MT assembly and stabilizes MTs *in vitro* and *in vivo*, by enhancing their rescue frequency (Nguyen *et al.,* 1999). Phosphorylation of Map4 modulates its MT stabilizing activity, reducing its affinity to bind MTs and affecting MT polymerization rate (Aizawa *et al.,* 1991; Chang *et al.,* 2001). Map4 is widely phosphorylated at mitosis in mammalian cells (Tombes *et al.,* 1991) and over the years several Cdk1-dependent phosphorylation sites have been identified within Map4 MTB but only serine 787 (S787) residue in the SPSK sequence showed an M-phase specificity, suggesting its critical role in regulating MT dynamics during mitosis (Ookata *et al.,* 1995; Ookata *et al.,* 1997; Kitazawa *et al.,* 2000). S787 sequence is conserved among mammalian species (West *et al.,* 1991),

supporting the relevance of its role in stabilizing MTs, alone or in combination with other phosphorylation sites.

Ch-Tog, a member of the Dis1/Tog MAP family (Charrasse *et al.,* 1998; Ohkura *et al.,* 2001; Kinoshita *et al.,* 2002) is the human homolog of *Xenopus l.* XMAP215 protein, that was originally isolated as a MAP with increasing MT growth rate properties (Gard *et al.,* 1987). As with many other MAPs, ch-Tog MT-stabilizing properties are regulated by cell cycle phosphorylation and ch-Tog is phosphorylated during mitosis. Cdk1-dependent phosphorylation inhibits promotion of MT elongation by ch-Tog, even if it has no significant effects on ch-Tog ability to bind MTs (Vasquez *et al.,* 1999). Nevertheless, ch-Tog colocalizes with MT plus ends and with centrosomes in mitotic cells (Gutiérrez-Caballero *et al.,* 2015; Lee *et al.,* 2001; Gergely *et al.,* 2003).

Therefore, Cdk1 phosphorylation and inhibition of stabilizing MAPs helps dissolution of interphase MT cytoskeleton. Nevertheless, the activity of MAPs is required for growth and stabilization of spindle MTs. Thus, how can these MAPs promote spindle MT growth while Cdk1 is at its highest activity level and exerts an antagonistic function? This is the unsolved question that I have tackled in this thesis.

IV. AIMS OF THE THESIS

IV. AIMS OF THE THESIS

Based on the previous observation that cdk1AF overexpression (Krek *et al.,* 1991b) offsets spindle assembly and that a small fraction of Cdk1 is inhibited by phosphorylation (i-Cdk1) in mitosis (D'Angiolella *et al.,* 2007; Oh *et al.,* 2011), we aim at dissecting whether and how i-Cdk1 was required in mitosis for spindle assembly (Figure 13).

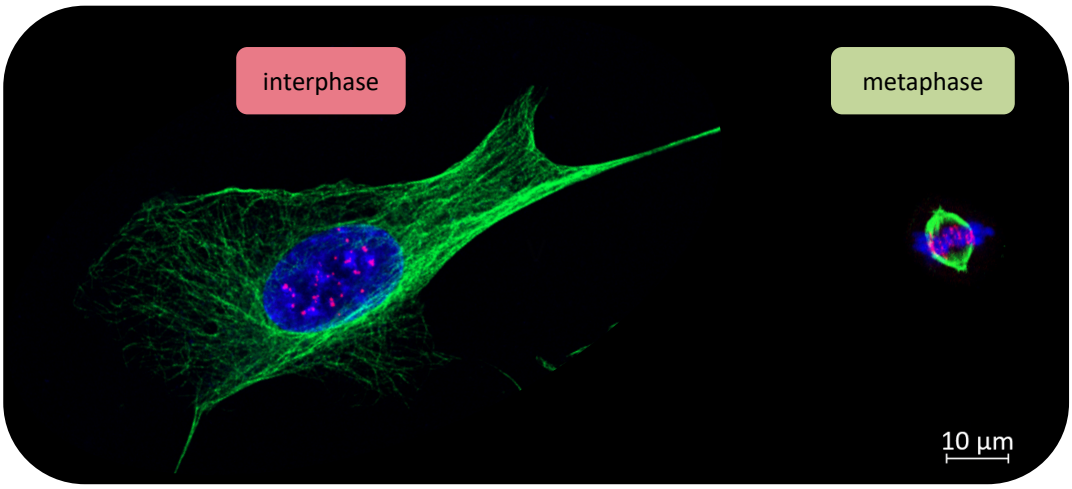

Figure 13 | Interphase and spindle MTs. HTERT-RPE1 cells fixed at interphase and metaphase, and stained for α-tubulin (green), CREST (red) and DNA (blue). Scale bar: 10 µm.

V. MATERIALS AND METHODS

V. MATERIALS AND METHODS

V.1 Cell lines and cell culture

HeLa cells were grown in Roswell Park Memorial Institute Medium (RPMI-1640; Sigma-Aldrich), HTERT-RPE1 cells were grown in Dulbecco's Modified Eagle Medium: Nutrient Mixture F-12 (DMEM/F12; Gibco, Thermo Fisher Scientific), both supplemented with 10% fetal bovine serum (FBS; Gibco), 1% GlutaMAX-supplement (Gibco), 1% penicillin/streptomycin (Euroclone), at 37° C with 5% CO_2.

V.2 Transfections and siRNAs

Transient expression transfections were performed using linear polyethylenimine (PEI; Polysciences, Inc.) or MegaTran 2.0 Transfection Reagent (OriGene Technologies, Inc.).

The expression plasmids for turbo-GFP-Map4-wild type (tGFP-Map4-WT), turbo-GFP-Map4 rendered non phosphorylatable at serine 787 (tGFP-Map4-S787A) and turbo-GFP-Map4 defective in PP1 binding to Map4 (tGFP-Map4-PP1-KO) were generated and purchased by OriGene Technologies Inc. To generate tGFP-Map4-S787A mutant version, serine (S) 787 residue of human Map4 was mutagenized into alanine (A) in tGFP-Map4 expression construct as template (OriGene Technologies Inc.). To generate tGFP-Map4-PP1-KO-mutant version, the Map4 peptide KDVRW (from aa 318 to 322) was mutated into KDARA (V $\rightarrow$ A; W $\rightarrow$ A). Wild type cdk1 (cdk1WT) and non phosphorylatable cdk1 mutant (T14A, Y15F; cdk1AF) expression plasmids were purchased from Addgene. 3XFlag-Wee1 expression construct was obtained as described (Visconti et al., 2012).

SiRNAs targeting the 3′-UTR of human Wee1 (5′-GGGCUUU AUUACAGACAUAUU-3′, 5′-GUACAUAGCUGUUUGAAAUUU-3′ and 5′-

UGUAAACUUGUAGCAUUAUU-3′) were purchased from Dharmacon Inc. For efficient knockdown cells were transfected with 25nM of siRNA duplex using DharmaFECT 1 siRNA Transfection Reagent (Dharmacon Inc.). For siRNA treatment and complementation experiments in synchronized cells, HeLa and HTERT-RPE1 cells were mock- or 3XFlag-Wee1 expression construct-transfected 24 hours prior to treatment with non-targeting or specific siRNAs.

V.3 Chemicals and treatments

For synchronization of siRNA-treated cells, 6 hours after siRNA-treatment, cells were incubated with RO-3306 (high-RO at 9 μM; Calbiochem) for further 16 hours of incubation, to have G2-arrested cells, or with nocodazole (Abcam) at 1 μg/mL and 100 ng/mL for further 14 or 12 hours of incubation for hTERT-RPE1 and HeLa cells, respectively, to have prometaphase-arrested cells (Pro cells). To obtain metaphase-arrested cells (Meta cells), Pro cells were collected and washed twice with fresh medium and twice with phosphate buffer saline (PBS; Euroclone) solution before plating into fresh medium containing MG-132 (20 μM; Calbiochem) and cycloheximide (CHX; 60 μg/mL; Santa Cruz Biotechnology, Inc.) for further 60 min incubation. Meta- and -Pro cells were obtained by adding either DMSO, as control, or nocodazole (1 μg/mL) to Meta cells at 60 min and prolonging incubation for further 20 min. Where indicated, AZD1775 (Selleckchem) was added at 1 μM. Where indicated, partial reversal of Cdk1 activity was obtained by adding RO-3306 at 0,5 μM (low-RO).

V.4 Antibodies

Antibodies used for immunoblotting (Ibs) according to standard protocols: mouse anti-cdc2 (1:500; BD Biosciences), rabbit anti-phospho-

tyrosine15-cdc2 (P-Y15-cdc2; 1:1000; Boster Bio), rabbit anti-phospho-threonine14-cdc2 (P-T14-cdc2; 1:1000; Cell Signaling Technology Inc.; CST), rabbit anti-Wee1 (1:1000; CST), rabbit anti-Myt1 (1:1000; CST), rabbit anti-Cdc25C (1:1000; CST), rabbit anti-phospho-threonine320-PP1α (P-T320-PP1; 1:1000; CST), rabbit anti-cyclin B1 (1:2000; Bethyl Laboratories, Inc.), mouse anti-γ-tubulin (1:2000; Sigma-Aldrich), mouse anti- α-tubulin (1:2000; Sigma-Aldrich), mouse anti-PP1γ (1:500; Santa Cruz Biotechnology, Inc.), rabbit anti-Map4 (1:2000; Bethyl Laboratories Inc.), rabbit anti-NuMA (1:1000; Novus Biologicals), rabbit anti-ch-Tog (1:1000; Abcam), mouse anti-turboGFP (1:2000; OriGene Technologies). Rabbit polyclonal antibody against phosphorylate serine 787 of human Map4 (P-S787-Map4) was raised using C-DAKAPEKRA[Sp]PSKPA-coNH2 peptide as immunogen; peptide synthesis, rabbit inoculation, serum production and cross-affinity antibody purification were carried out by CovalAb S.A.S. Sheep anti-mouse IgG peroxidase-(HRP) linked and donkey anti-rabbit IgG HRP-linked whole antibodies (1:2000; GE Healthcare).

Antibodies used for indirect immunofluorescence (IF): rabbit anti-phospho-tyrosine15-cdc2 (P-Y15-cdc2; 1:50; CST), anti-cdc2 (1:100; BD Biosciences), mouse anti-γ-tubulin (1:1000; Sigma-Aldrich), mouse anti-α-tubulin (1:1000; Sigma-Aldrich), rabbit anti-γ-tubulin (1:1000; Sigma-Aldrich), human anti-centromere (CREST; 1:50; Antibodies Incorporated), rabbit anti-Map4 (1:1000; Abcam), rabbit anti-ch-Tog (1:400; Proteintech Group, Inc.), rabbit anti-Wee1 (1:100; CST), goat anti-human IgG rhodamine conjugated (4 µg/mL; Santa Cruz Biotechnology, Inc.), rabbit anti-human IgG FITC conjugated (4 µg/mL; Dako Agilent), Alexa Fluor 594 donkey anti-rabbit IgG (2 µg/mL; Invitrogen), Alexa Fluor 594 donkey anti-mouse IgG (4 µg/mL; Invitrogen), Alexa Fluor 488 donkey anti-rabbit IgG (2 µg/mL; Invitrogen), Alexa Fluor 488 goat anti-mouse IgG (4 µg/mL; Invitrogen).

Antibodies used for immunoprecipitations (Ips): rabbit anti-Map4 (2 μg/mL; Bethyl Laboratories Inc.), rabbit anti-ch-Tog (2 μg/mL; Abcam), mouse anti-γ-tubulin (2 μg/mL; Sigma-Aldrich).
Antibody-conjugated beads for Ips: mouse anti-cyclin B1 agarose (15 μL of 25% suspension; Santa Cruz Biotechnology, Inc.), mouse anti-turboGFP agarose (10 μL of 50% suspension; OriGene), protein A/G PLUS-agarose (15 μL of 25% suspension; Santa Cruz Biotechnology), mouse anti-γ-tubulin agarose conjugated (15 μL of 25% suspension; Santa Cruz Biotechnology).

V.5 Cell fractionation and extracts

To isolate spindle-bound proteins we adapted a previously described method (Silljé *et al.,* 2006). All the steps, except the final elution, were performed at room temperature (rt) to preserve MT conformations. Cells were harvested by centrifugation and washed once with PBS containing paclitaxel (1 μM; Sigma-Aldrich). 5 x 10^6 cells were resuspended in 800 μL of fractionation lysis buffer (FLB; 40 mM β-glycerophosphate, 15 mM $MgCl_2$, 20 mM EGTA, 0,25% Igepal, 5 mM Hepes, 5 μM paclitaxel; 6 μg/mL latrunculin B; Sigma-Aldrich) supplemented with 300 μg/mL RNase and 120 U/mL DNase I (Roche). After careful resuspension, samples were incubated in thermomixer at 34 °C for 20 min with constant shacking at 1,200 rpm (Eppendorf thermomixer comfort). Lysates were spun at 6,800 rpm for 2 min (Eppendorf centrifuge 5425): the supernatant fractions were collected and transferred into new tubes with the addition of 250 mM NaCl (S fraction) to enhance protein solubilization, while the pellet fractions were resuspended in FLB + 300 μg/mL RNase and 120 U/mL DNase I and again incubated in thermomixer at 34 °C for 20 min with constant shacking at 1,200 rpm (Eppendorf thermomixer comfort). Lysates were collected again by centrifugation and the pellets were washed twice with washing buffer (WB; 5 mM Hepes, 5 μM paclitaxel; Sigma-Aldrich). Finally, the pellet fractions were resuspended in 180 μL FLB minus

paclitaxel supplemented with 250 mM NaCl (P fractions). Both S and P fractions were incubated on ice for 30 min, to help MT destabilization, and then spun by centrifugation at 13,200 rpm at 4 °C for 10 min (Eppendorf centrifuge 5424 R). The supernatants of S and P fraction were further analyzed by Ibs or Ips.

To induce MT polymerization and analyze MT-bound proteins in mitotic cell extracts, HeLa cell extracts were obtained as previously described (Visconti *et al.,* 2012). Cell extracts were supplemented with 1 mM guanosine-5'-triphosphate (GTP; Sigma-Aldrich), 50 µL aliquots were treated with nocodazole (1 µg/mL; Abcam), as control, or paclitaxel (5 µM; Sigma-Aldrich) for 20 min at rt, diluted 10 times with FLB and spun at 6,800 rpm for 2 min (Eppendorf centrifuge 5425). The pellets were washed once more in FLB and finally resuspended in 30 µL FLB supplemented with 250 mM NaCl, incubated on ice for 30 min and then spun at 13,200 rpm at 4 °C for 10 min (Eppendorf centrifuge 5424 R). Supernatants were analyzed by Ibs; total samples = 5 µL of total mitotic extract.

V.6 *In vitro* phosphorylation and dephosphorylation assays

For kinase reaction, after two lysis buffer (LB; 80 mM β-glycerophosphate, 15 mM MgCl2, 20 mM EGTA, 20 mM Hepes pH 7.4, 100 mM NaCl, 0,1 % Igepal; Sigma-Aldrich) washes, Ips were washed once in kinase reaction buffer (KRB; 80 mM β- glicerophosphate, 15 mM $MgCl_2$, 20 mM EGTA, 20 mM Hepes pH 7.4, 100 µM ATP; Sigma-Aldrich) and incubated for 20 min at 37 °C in KRB -/+ recombinant human active Cdk1 (0.05 mg/mL; Sigma-Aldrich) and + active Cdk1 + RO-3306 (10 µM). For phosphatase reactions, after two LB washes, Ips were washed once in phosphatase reaction buffer (PRB; 20 mM Hepes pH 7.4, 150 mM NaCl, 1 mM DTT, 1 mM $MnCl_2$; Sigma-Aldrich) and incubated in PRB -/+ 0.01 mg/mL recombinant human PP1α (Novus Biologicals) for 20 min at 30 °C.

V.7 Immunoblotting and immunoprecipitation

Ibs were performed as described (Serpico *et al.,* 2019).
For Ips from S fraction and P fraction eluates, samples were diluted 6 folds in LB supplemented with 1 tablet of phosphatase inhibitor cocktail (PhosSTOP; Roche) and incubated with antibody and protein A/G PLUS-agarose beads or with agarose bead-conjugated antibody overnight at 4 °C in constant rotation. Beads were washed twice in LB and beads-bound proteins were eluted by boiling in SDS loading buffer. For total cell lysates, 5 x 10^6 cells were lysed in 180 µL high salt lysis buffer (HSB; 16 mM β-glycerophosphate, 3 mM $MgCl_2$, 4 mM EGTA, 0,5 mM DTT, 20 mM Hepes, 0,5% Igepal, 250 mM NaCl; Sigma-Aldrich) supplemented with 1 tablet of phosphatase inhibitor cocktail (PhosSTOP; Roche) to preserve phosphorylation. After 30 min incubation on ice, lysates were spun at 13,200 rpm for 10 min at 4 °C (Eppendorf centrifuge 5424 R). Cleared lysates were incubated with the antibody and protein A/G PLUS-agarose beads or with agarose bead-conjugated antibody overnight at 4 °C in constant rotation. Beads were washed twice in LB and beads-bound proteins were eluted by boiling in SDS loading buffer.

V.8 Immunofluorescence staining and microscopy

Cells were grown onto poly-D-lysine (0,1 mg/mL; Sigma-Aldrich) coated glass coverslips and treated as described in the text. Before IF procedure initiation, coverslips were washed twice with PBS, then cells were fixed with 4% paraformaldehyde (PFA; Sigma-Aldrich) in PBS (Euroclone) for 10 min at rt and with a methanol (99,9%; Exacta + Optech) additional step at -20° C for 10 min, the latter except for α-tubulin staining. Cells were permeabilized with 0,25-0,5% Triton X-100 (Sigma-Aldrich) in PBS for 15-30 min, washed once with PBS and incubated with 3% bovine serum albumin (BSA; Sigma-Aldrich) in PBS for 1 hour at rt. Coverslips were transferred into a humidity chamber

and incubated with primary antibodies in 1,5% (w/v) BSA-PBS solution for 2-12 h at 4° C. Samples were washed three times and incubated with fluorescently labelled secondary antibodies, dissolved in 1,5% BSA-PBS solution, for 1 hour at rt. DNA was stained with Hoechst 33258 (1 μg/mL; Invitrogen) by incubation for 10 min. Finally, samples were washed four times and mounted with Mowiol 40-88 (Sigma-Aldrich) on a glass side. Fixed cells were observed using a LSM 980 inverted confocal microscope (Zeiss) with a 63X/1,4 oil objective. Representative images were obtained collecting 3 Z-stack series over 42 μm. The acquisitions were deconvoluted and projected into one plane using the LAS-AF software.

V.9 Statistics and reproducibility

For quantitative analyses of IF experiments investigators were blinded to sample allocation. Metaphases were visually scored and those with more than three chromosomes falling outside the two internal quarters of the interpolar distance were considered misaligned; around 100 cells were scored in 4 fields of each slide for each experimental condition; each experiment was repeated 3-5 times with similar results.

VI. RESULTS

VI. RESULTS

VI.1 Preventing Cdk1 inhibitory phosphorylation in mitosis affects spindle assembly

To assess whether Cdk1 inhibitory phosphorylation plays a role for spindle assembly, we analyzed spindle formation through indirect immunofluorescence (IF) upon downregulation of Wee1 expression by small interfering RNAs (siRNAs) in hTERT-RPE1 cells. 6 hours from Wee1-siRNA treatment, cells were further incubated with the selective and reversible Cdk1 inhibitor RO-3306 at 9 μM (high-RO) for 16 hours to arrest cell cycle at G2 and allow DNA replication completion, thus preventing premature mitosis onset upon Wee1 downregulation (Wee1 depletion reached 90% by the end of this period; Figure 14a) (Vassilev *et al.,* 2006; Visconti *et al.,* 2015). Part of Wee1-siRNA-treated cells were complemented with a siRNA-resistant Wee1 expression plasmid and used as control cells. (Figure 14a) (Visconti *et al.,* 2015). G2-arrested cells were released in fresh medium containing the proteasome inhibitor MG-132 to block protein degradation and mitosis exit and the protein synthesis inhibitor cycloheximide (CHX) to prevent abnormal protein accumulation (M/C medium). Under this condition the majority of control cells built normal bipolar spindles within 60 min incubation and preserve this phenotype for further 20 min incubation (Figure 14b). Conversely, under the same incubation times, Wee1-downregulated cells exhibited defective spindle assembly, comprising monopolar spindle conformations and loosely structured bipolar spindles with evident chromosome alignment abnormalities (Figure14b).

To establish whether impaired spindle assembly was due to Wee1 loss *per se* or to loss of Wee1-dependent inhibitory control of Cdk1, we asked if mild inhibition of Cdk1 activity in Wee1-downregulated cells could restore normal spindle assembly. Indeed, adding RO-3306 at 0,5 μM (low-RO) from 60 to 80

min post G2 release to Wee1-siRNA-treated cells restored bipolar spindle assembly in most mitotic cells (Figure 14b).

In another set of experiments, non-targeting-siRNA-, as control, and Wee1-siRNA-treated hTERT-RPE1 cells were synchronized at prometaphase with the reversible MT inhibitor nocodazole, added 6 hours post siRNAs treatment (as described in Materials and Methods section). Then, cells were released in M/C medium for 60 minutes (Figure 14c). At this time, a part of Wee1-downregulated cells received low-RO to partially inhibit Cdk1 activity. Overall, cells incubation lasted up to 80 minutes. Within this period, the majority of control cells showed correct spindles formation, Wee1-siRNA-treated cells exhibited deep abnormalities in spindle assembly that were largely rectified by low-RO addition (Figure 14c).

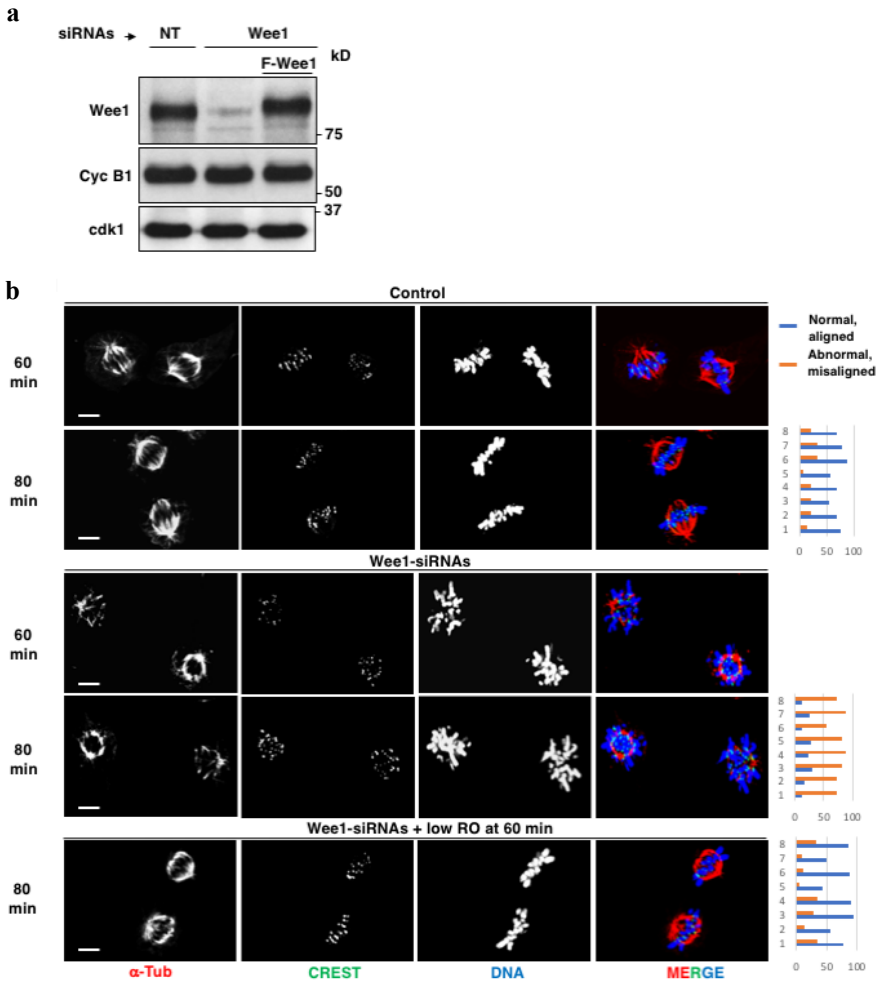

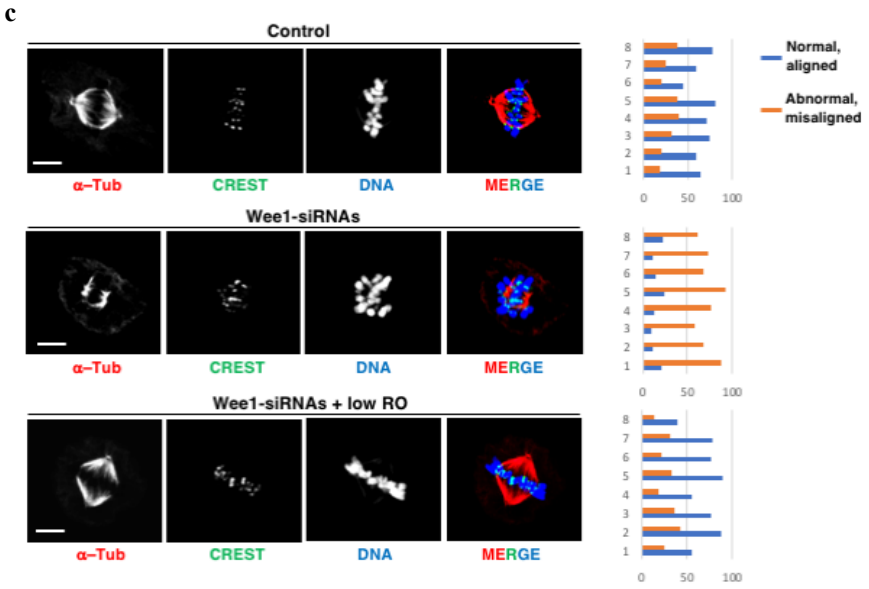

Figure 14 | Spindle assembly is affected by Wee1 downregulation. a, Lysates of hTERT-RPE1 cells treated with non-targeting-siRNAs (NT), with Wee1-siRNAs (Wee1) and with Wee1-siRNAs post siRNA-resistant, Flag-tagged Wee1 expression plasmid transfection (F-Wee1) were probed for indicated antigens. **b**, hTERT-RPE1 cells were synchronized at G2 phase by high-RO treatment, released and fixed at 60 and 80 min of incubation in M/C medium (see Materials and Methods section). Control: Wee1-siRNA-treated cells previously transfected with siRNA-resistant Wee1 expression plasmid; Wee1-siRNAs: Wee1-siRNA-treated cells previously transfected with empty plasmid; Wee1-siRNAs + low RO: Wee1-siRNAs plus low-RO adding at 60 min upon G2-arrest release. **c**, hTERT-RPE1 cells were synchronized at prometaphase with nocodazole, released and fixed after 80 min of incubation in M/C medium (see Materials and Methods section). Control: non-targeting-siRNA-treated cells; Wee1-siRNAs: Wee1-siRNA-treated cells; Wee1-siRNAs + low RO: Wee1-siRNAs plus low-RO adding at 60 min upon prometaphase-arrest release. Cells were stained for α-Tub (α-tubulin; red), CREST (centromere marker; green) and DNA (blue). Addition of vehicle (DMSO) had no effect in spindle assembly in Wee1-siRNA-treated cells. Graphs: quantitation of cells containing normal (aligned; blue bar) or abnormal (misaligned; orange bar) spindles at 80 min of incubation. Data shown are from two independent experiments (1-4, experiment 1; 5-8, experiment 2); around 100 cells were scored in 4 independent microscopy slide fields. Scale bar: 5 μm.

Conforming with Krek and Nigg observations from 1991, abnormalities in spindle assembly were also induced by overexpression of a non phosphorylatable mutant of cdk1 (cdk1AF) under similar conditions of G2-arrest and release (Krek *et al.,* 1991). hTERT-RPE1 cells were transfected with plasmids expressing wild type cdk1 (cdk1WT) or cdk1AF (Figure 15c) and 6

hours post transfection cells were synchronized at G2 by high-RO addition for further 16 hour incubation. By 80 minutes of incubation in M/C medium upon release from G2 arrest the majority of cells overexpressing cdk1WT assembled bipolar spindles, that remained stable for the next 20 minutes (Figure 15a). Contrarily, cdk1AF overexpression markedly impaired in proper spindle formation and caused cells to assemble monopolar or aberrant spindles with chromosome mis-segregation (Figure 15b). Partial inhibition of cdk1 activity by low-RO addition to cdk1AF overexpressing cells, at 60 minutes post G2 release, restored bipolar spindle assembly within 20 minutes (Figure 15b).

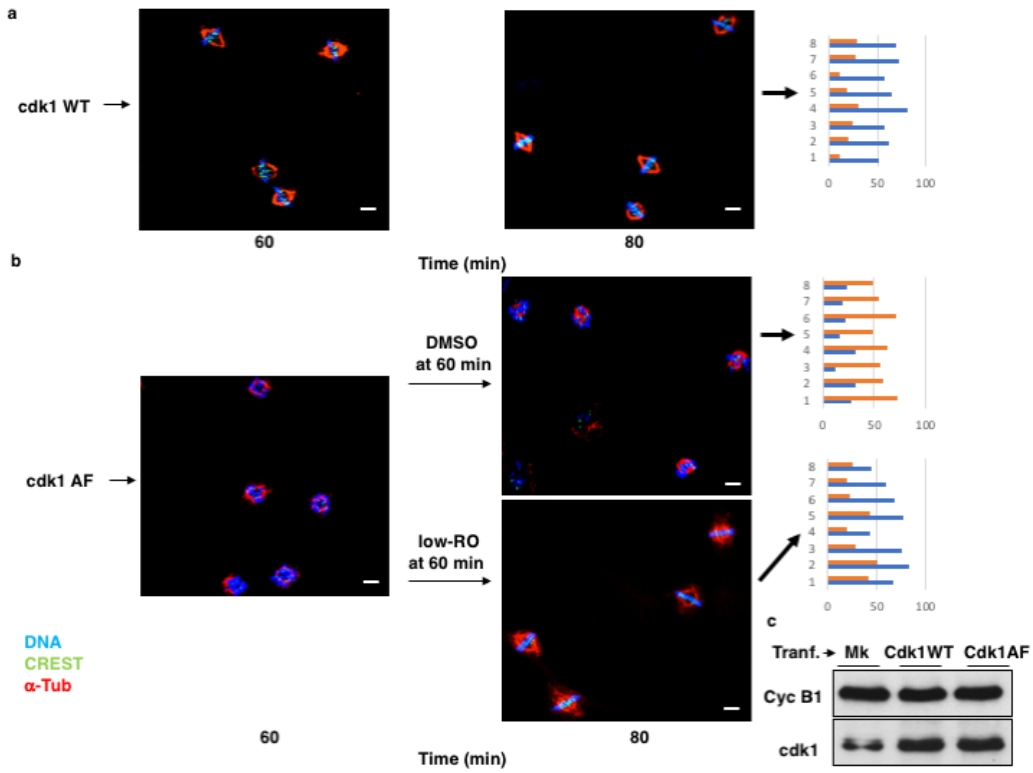

Figure 15 | Expression of a non phosphorylatable version of Cdk1 impairs spindle assembly. hTERT-RPE1 cells were transfected with **a**, wild type cdk1 (cdk1WT) or **b**, a mutant cdk1 (cdk1AF). 6 hours post transfection, cells were arrested at G2 by high-RO treatment. Cells were fixed and stained for DNA (blue), CREST (green) and α-Tub (red) at 60 and 80 min upon release from G2 arrest. A portion of cdk1AF-treated cells received low-RO at 60 min; as control vehicle (DMSO) was added. Graphs: quantitation of cells containing normal (aligned; blue bar) or abnormal (misaligned; orange bar) spindles at 80 min incubation. Data shown are from two independent experiments, in which around 100 cells were scored in 4 independent microscopy slide

fields (1-4, experiment 1; 5-8, experiment 2). Scale bar: 5μm. **c**, samples of cells treated as in **a**, and **b**, were lysed prior to release and probed for indicated antigens.

A result consistent with those described above was obtained by chemical inhibition of Wee1 via AZD1775 (Serpico *et al.,* 2019). hTERT-RPE1 cells were synchronized at G2 by high-RO treatment, released into M/C medium and treated with either vehicle (DMSO; Control) or AZD1775 for 80 minutes (Figure 16). Control cells assembled mitotic spindles while those treated with AZD1775 failed to form bipolar spindles. Partially interfering with Cdk1 activity by low-RO addition to AZD1775-treated cells almost completely restored spindles bipolarity (Figure 16).

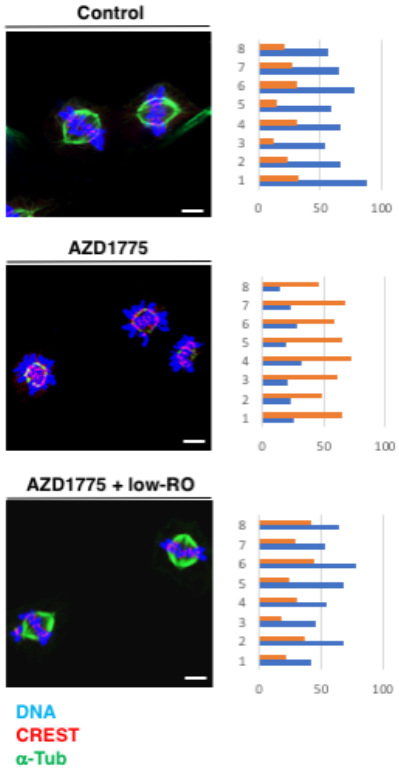

Figure 16 | Spindle assembly is affected by chemical inhibition of Wee1. hTERT-RPE1 cells were synchronized at G2 phase by high-RO treatment and released into M/C medium (see Materials and Methods section) and either vehicle (DMSO; Control) or AZD1775 was added. A portion of AZD1775-treated cells also received low-RO 60 min post release. Cells were fixed after further 80 min of incubation and stained for DNA (blue), CREST (red) and α-Tub (green). Scale bar: 5μm. Graphs:

quantitation of cells containing normal (aligned; blue bar) or abnormal (misaligned; orange bar) spindles at 80 min incubation.

Together, these data suggest that inhibitory control of Cdk1 activity by Wee1-dependent phosphorylation is required for proper spindle assembly.

VI.2 I-Cdk1 is spindle structure-bound

To directly know if and where i-Cdk1 was present in mitotic cells, we performed an IF in metaphase arrested hTERT-RPE1 and HeLa cells. Growing cells were treated with MG-132 for 20 minutes, fixed and probed with an antibody recognizing cdk1 phosphorylated at tyrosine 15 (p-Y15-cdk1; Figure 17). The p-Y15-cdk1 signal appeared to decorate the spindle area paralleling total cdk1 localization (Figure 17).

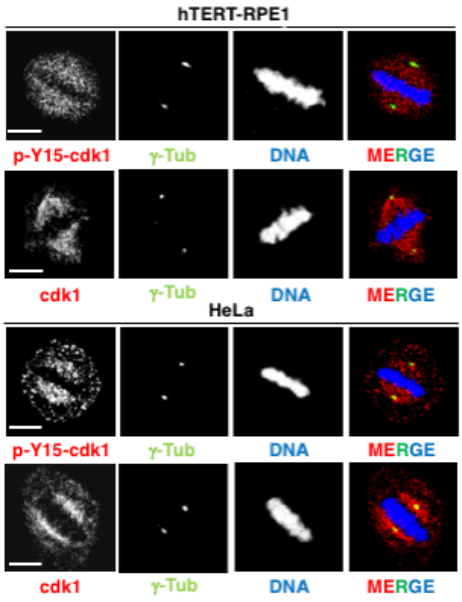

Figure 17 | I-Cdk1 localizes at spindle structures. Growing hTERT-RPE1 and HeLa cells were treated for 20 min with MG-132, fixed and stained for indicated antigens (γ-Tub: γ-tubulin). Scale bar: 5μm.

To biochemically dissect the localization of i-Cdk1, we adopted and adjusted a method described by Nigg and co-workers (Silljé *et al.,* 2006) to isolate mitotic

spindles and associated proteins by separating microtubular and insoluble pellet fraction (P) from the cytosolic and soluble supernatant fraction (S) (see Materials and Methods section). Prometaphase-arrested hTERT-RPE1 cells were collected and taken at time 0 (Pro) or taken after release in M/C medium for 60 minutes to gain metaphase-synchronized cells (Meta). Cells were fractionated and proteins from S and P fractions analyzed (Figure 18a). (The P fraction was enriched 4 folds compared to the S fraction). Key centrosome- and MTOC-associated proteins, γ-tubulin and NuMA1, were present at comparable levels both in Pro and Meta cells P fractions (Figure 18a). Conversely, α-tubulin distribution differed profoundly between P fractions of Pro and Meta cells, reflecting polymerization of spindle MT. Indeed, α-tubulin was substantially present in S fraction of Pro cells and much less in relative P fraction, as further proof of the chemical block to MT polymerization induced by nocodazole treatment. Paralleling α-tubulin distribution, the MAPs Map4 and ch-Tog preponderated in Pro cells S fraction compared to P fraction (Figure 18a). Oppositely, in Meta cells α-tubulin and significant amounts of Map4 and ch-Tog were present in P fraction, reflecting MT polymerization and spindle assembly (Figure 18a). Meta cells P fraction also contained small amounts of Wee1, that were even less noted in Pro cells P fraction. Minimal amounts of Cdc25C were equally present in P fractions of both Pro and Meta cells (Figure 18a). Cyclin B1 and cdk1 were present in small amounts in P fraction of Pro cells and in slightly larger amounts in P fraction of Meta cells (Figure 18a). I-Cdk1, however, was found quite exclusively in P fractions, with a prevalence in Meta relatively to Pro cells, as shown by retarded Cdk1 mobility on SDS/PAGE and confirmed by p-Y15-cdk1 signal detection (Figure 18a). As indicated by densitometric quantitation of the upshifted cdk1 forms from Meta cell P fraction, i-Cdk1 represents less than 10% of total cdk1 content. Similar protein distribution was found in HeLa cells under similar experimental conditions (data not shown). We also performed immunoprecipitations (Ips) of comparable amounts of cyclin B1 from Meta

cells S and P fractions to confirm the selective presence of i-Cdk1 in P fraction (Figure 18c). Another important piece of information we got from fractionating Meta cells content concerns Map4 and ch-Tog putative phosphorylation status (Figure 18a). Map4 and ch-Tog in P fraction of Meta cells seemed to have increased mobility on SDS/PAGE compared to the S fraction, suggesting these proteins were relatively dephosphorylated when associated to MTs. Indeed, when Meta cells were further treated to revert to a prometaphase condition, via nocodazole adding from 60 to 80 minutes post chromosome congression at metaphase plate, Map4 and ch-Tog reverted to a prometaphase distribution (Figure 18b). On the whole, distribution of all proteins between S and P fractions returned similar to Pro cells and Map4 and ch-Tog in S fraction regained slower migration on SDS/PAGE, presumably reflecting their re-phosphorylation. Moreover, Wee1 and i-Cdk1 amounts were reduced in P fraction, implying their dependence also on MT polymerization status (Figure 18b).

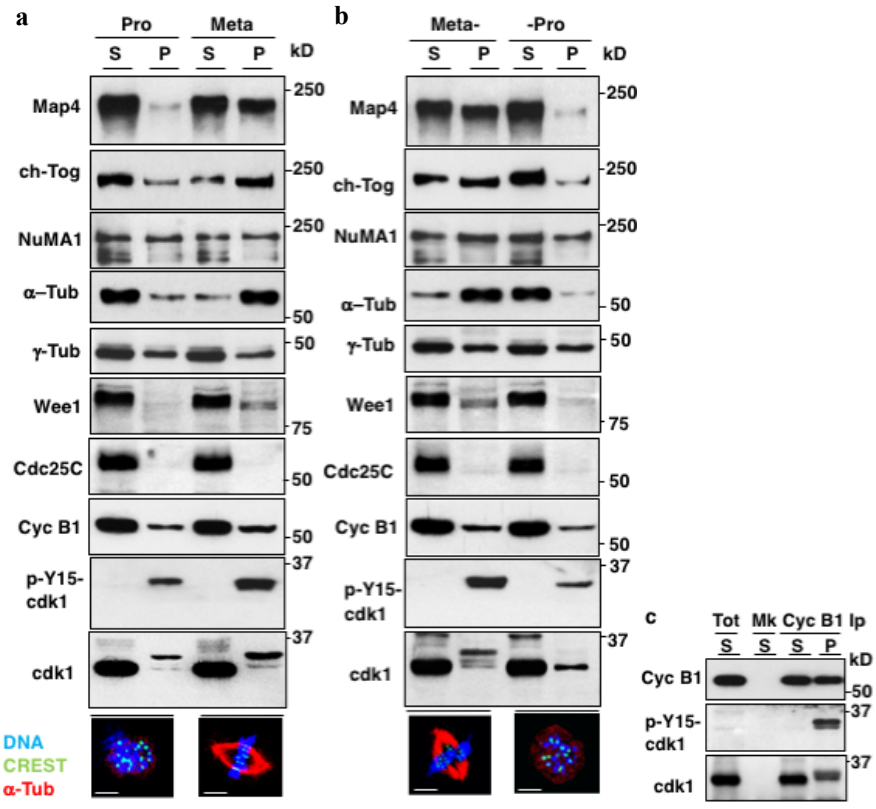

Figure 18 | Spindle assembly requires localized i-Cdk1. a, Prometaphase-arrested hTERT-RPE1 cells were released in M/C medium for 60 min and either nocodazole (Pro) or just vehicle (DMSO; Meta) were added at time 0 of incubation. S and P fractions were probed for indicated antigens. At the bottom, samples of Pro and Meta hTERT-RPE1 cells were fixed and stained for indicated antigens. **b**, Meta cells obtained as described in **a**, were further treated with vehicle (DMSO; Meta-) or nocodazole (-Pro) from 60 min to 80 min of incubation. S and P fractions were probed for indicated antigens. At the bottom, samples of Pro and Meta hTERT-RPE1 cells were fixed and stained for indicated antigens. **c**, Meta cell S and P fractions were processed for Cyclin B1 (Cyc B1) Ips and probed for indicated antigens.

VI.3 I-Cdk1 is required for MT-stabilizing MAP association to spindle MTs

To assess a cause-effect relationship between i-Cdk1 and Map4 and ch-Tog dephosphorylation and distribution, we analyzed these proteins in cell fractionation experiments upon Wee1 expression downregulation. Control and Wee1-siRNA-treated cells were synchronized at prometaphase and release into M/C medium as described in Figure 14c. Cells were further fractionated and resulting S and P fractions were analyzed (Figure 19a). Control cells showed protein fractionation matching that described for Meta cells in Figure 18a, b. In Wee1-siRNA-treated cells γ-tubulin and NuMA1 distribution between S and P fractions was similar to control cells. Contrarily, Map4, ch-Tog and even α-tubulin were less present in the P fractions of Wee1-siRNA-treated cells compared to control cells, a distribution pattern resembling that found in Pro cells described in Figure 18a, b (Figure 19a). Spindle assembly restoration in Wee1-siRNA-treated cells via low-RO addition reversed protein distribution relocating Map4, ch-Tog and α-tubulin from S to P fractions similarly to control cells (Figure 19a). As expected, i-Cdk1 amount was reduced in Wee1-downregulated cell P fraction compared to control, as supported by lowered p-Y15-cdk1 detection. However, addition of low-RO restored i-Cdk1 content and induced localization of part of residual Wee1, escaping siRNA-mediated downregulation, in P fraction. (Figure 19a; note Wee1 in short, SE, and long exposures, LE). Moreover, low-RO adding did not induce any p-Y-15-cdk1

signal increase in S fraction, suggesting that small fluctuations of Cdk1 activity are buffered in the cytosol by hysteresis and bi-stability of Cdk1 auto-activatory loops, while centrosome-nucleating MTs were separated from these loops and were subjected to different regulatory mechanisms (Figure 19a) (Pomerening *et al.,* 2003; Hunt, 2013; Novák *et al.,* 2021). Similarly, restoration of spindle assembly in cdk1AF-expressing cells by low-RO treatment (see Figure 15b) could be possibly explained as a result of localized inhibition of endogenous Cdk1. Map4 and ch-Tog altered MT localization upon Wee1 downregulation was confirmed by IF (Figure 19b). The defectively structured spindles in Wee1-siRNA-treated cells showed a reduced localization of the two MAPs compared to the control cells. Low-RO addition restored proper spindle assembly and induced Map4 and ch-Tog to regain a normal spindle accumulation (Figure 19b).

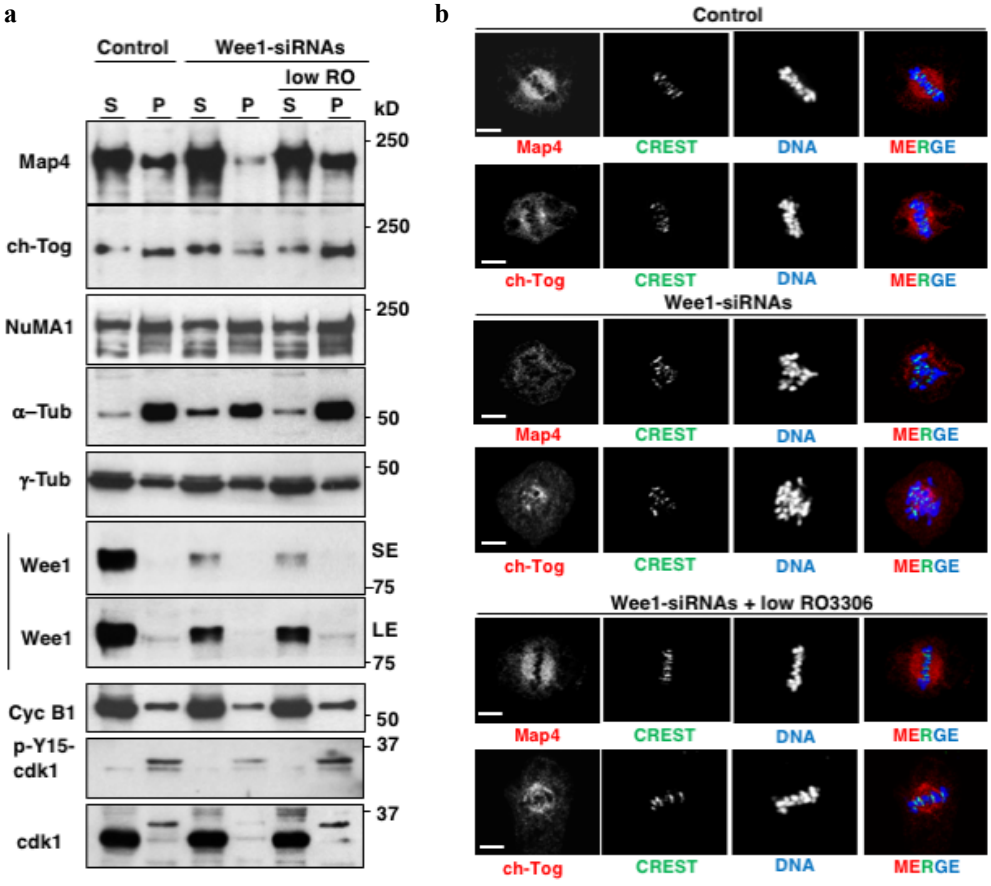

Figure 19 | Wee1 downregulation alters spindle protein distribution. a, **b**, hTERT-RPE1 cells were treated with non-targeting-siRNAs (Control) and Wee1-siRNAs (Wee1-siRNAs), arrested at prometaphase and released in M/C medium for 80 min incubation as described in Figure 14c and a portion of Wee1-siRNA-treated cells received low-RO at 60 min post release. **a**, S and P fractions were probed for indicated antigens. **b**, Cells were fixed and stained for indicated antigens. Scale bar: 5μm.

Chemical Wee1 inhibitor AZD1775 treatment of prometaphase-arrested cells induced similar mitotic defects and altered protein pattern distribution to those caused by Wee1-siRNA-induced downregulation, also in this case reversible in a low-RO addition (Figure 20).

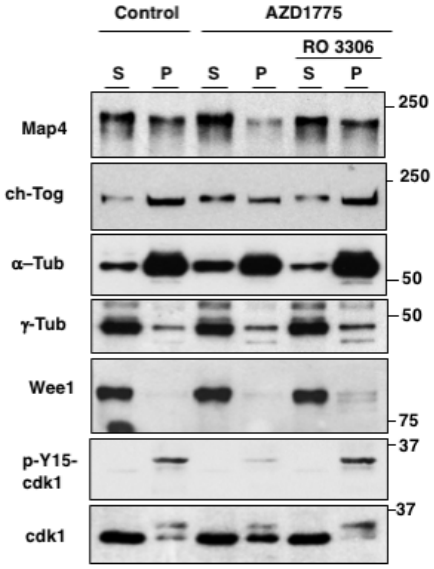

Figure 20 | Chemical inhibition of Wee1 alters spindle protein distribution. Prometaphase-arrested hTERT-RPE1 cells were released into M/C medium and either vehicle (DMSO; Control) or AZD1775 was added. A portion of AZD1775-treated cells also received low-RO 60 min post release. S and P fraction were prepared after 80 min of incubation and probed for indicated antigens.

Together, these data indicate that the i-Cdk1 pool persisting during mitosis is required for proper spindle assembly and provides conditions suitable for spindle MT association of stabilizing MAPs, like Map4 and ch-Tog.

VI.4 I-Cdk1 drives PP1-dependent MAP dephosphorylation

To directly investigate whether MAPs were dephosphorylated at Cdk1-dependent sites when bound to MTs, we developed an anti-phosphospecific antibody recognizing phosphorylated Map4 serine 787 (p-S787-Map4), a target site for inhibitory phosphorylation by Cdk1 *in vivo* (Ookata *et al.,* 1997). To validate antibody specificity, plasmids carrying either Map4 wild type form (tGFP-Map4-WT) or Map4 mutant version, in which serine 787 was mutated into non-phosphorylatable alanine (tGFP-Map4-S787A), were expressed in hTERT-RPE1 cells and the fusion proteins were isolated after prometaphase synchronization (Figure 21a). As expected, the p-S787-Map4 specific antibody recognized wild type Map4 but not the mutant version (Figure 21a). Ips of comparable amounts of endogenous Map4 from S and P fractions of Meta cells were probed for p-S787-Map4 and the signal was readly detected from S fraction while hardly from P fraction (Figure 21b). In addition, P fraction Map4 pool treated with active Cdk1 *in vitro* regained strong phosphorylation at S787 and slower migration on SDS/PAGE (Figure 21c). These data indicate that Map4 is dephosphorylated at least at one Cdk1-dependent site when bound to MTs.

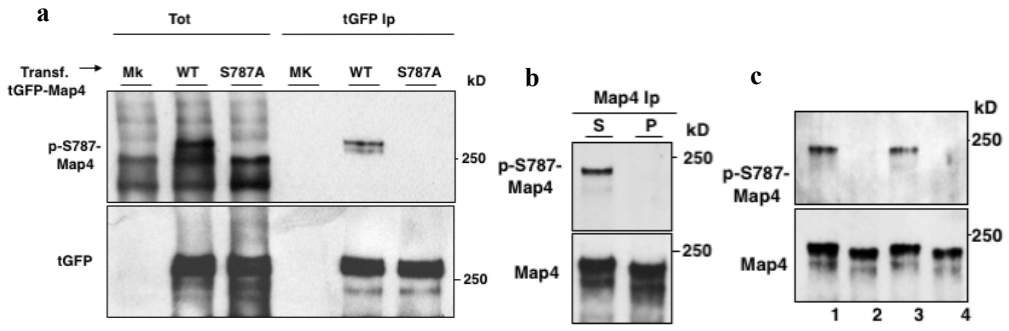

Figure 21 | Spindle-bound Map4 is dephosphorylated at Cdk1-dependent site. a, hTERT-RPE1 cells were transfected with expression plasmids of tGFP-Map4 wild type (WT) or tGFP-Map4 non phosphorylatable mutant at serine 787 (S787A) and arrested at prometaphase. Total cell lysates (Tot) and relative anti-tGFP Ips were probed for indicated antigens (MK: mock-transfected cells). **b**, S and P fractions of Meta hTERT-RPE1 cells were processed for Map4 Ips and probed for indicated

antigens. **c**, Map4 Ips from S and P fractions of Meta hTERT-RPE1 cells were incubated in kinase reaction buffer for 15 min at 37° C: lane 1, from S fraction; lanes 2, 3, 4, from P fraction – active Cdk1, + active Cdk1, + active Cdk1 + RO-3306, respectively. After incubation, Ips were probed for indicated antigens.

Our data from Wee1 downregulation experiments indicated that Map4 and ch-Tog distribution in the P fraction of mitotic cells relied on i-Cdk1 pool. These MAPs have been shown to physically interact with Cdk1, mediating its association with MTs (Ookata *et al.,* 1995; Charrasse *et al.,* 2000). We isolated comparable amounts of Map4 and ch-Tog from S and P fractions of Meta cells and we found only P fraction MAPs pool interacted selectively with i-Cdk1 (Figure 22a, b). Together, these observations suggest that the binding of MT-associated MAPs to i-Cdk1 was instrumental for their dephosphorylation (Figure 22a, b). In mitosis, Cdk1 directly or indirectly inhibits major protein phosphatases like PP1s and PP2As (Hégarat *et al.,* 2016; Qian *et al.,* 2013). PP1 catalytic subunit is directly inhibited by Cdk1 phosphorylation, in particular at threonine 320 in alpha isoform (p-T320-PP1α) and at analogous sites in other PP1 isoforms (Kwon *et al.,* 1997; Dohadwala *et al.,* 1994). PP1 can, however, activate by auto-dephosphorylation in the absence of Cdk1 activity (Kwon *et al.,* 1997). Moreover, PP1 phosphatases often interact with their substrates through specific domains (Meiselbach *et al.,* 2006; Hendrickx *et al.,* 2009; Heroes *et al.,* 2013). Thus, we asked whether mitotic spindle-associated Map4 and ch-Tog, that we had found relatively dephosphorylated, interacted with PP1. Indeed, these MAPs isolated from Meta cells were bound to PP1α only in the P fraction (Figure 22a, b).

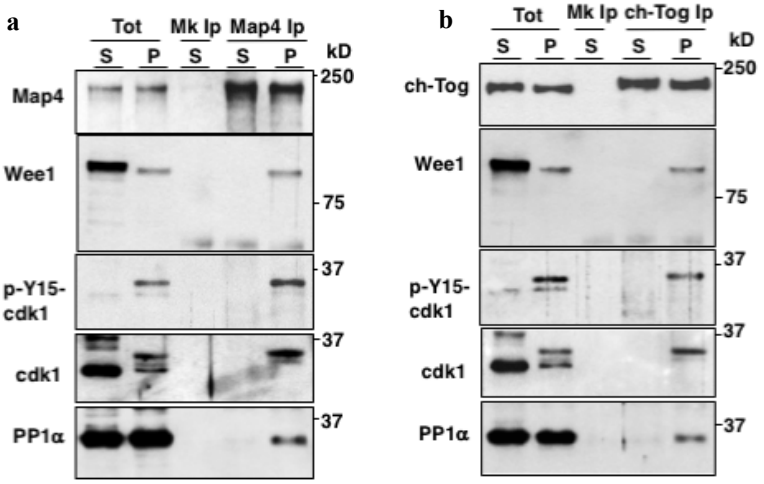

Figure 22 | Spindle-bound MAPs selectively interact with i-Cdk1 and PP1. a, **b**, S and P fractions of Meta hTERT-RPE1 cells were processed for **a**, Map4 and **b**, ch-Tog Ips and probed for indicated antigens.

Because of the presence of i-Cdk1, we hypothesized that PP1α present in P fraction could be less phosphorylated at its Cdk1-dependent inhibitory site compared to that in S fraction. Thus, we analyzed comparable amounts of PP1α from S and P fractions of Meta cells and we found the p-T320-PP1 signal readly detected in S fraction but hardly in the P fraction (Figure 23a). In addition, we found that MAP-associated PP1α was dephosphorylated at T320. (Figure 23b). Moreover, recombinant active human PP1α was able to dephosphorylate p-S787 of Map4 isolated from S fraction *in vitro* (Figure 23c). These data indicate that i-Cdk1 in the P fraction helps locally PP1 reactivation to reverse Map4 and ch-Tog inhibitory phosphorylation.

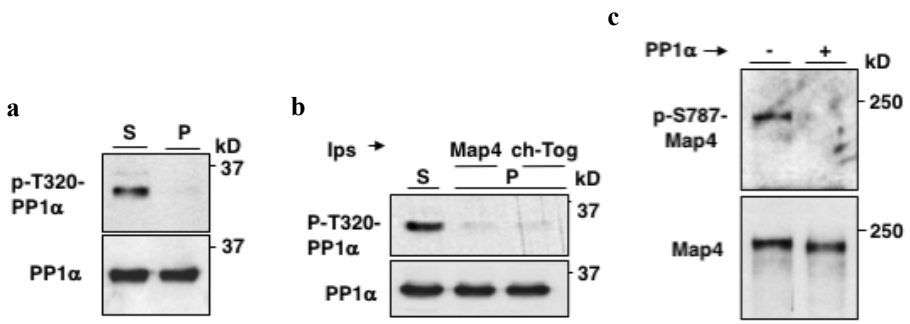

Figure 23 | Spindle-bound MAPs interact with locally active PP1. From Meta hTERT-RPE1 cells: **a**, S and P fractions were probed for indicated antigens. **b**, Total S

fraction (S) and Map4 and ch-Tog Ips from P fraction (P) were probed for indicated antigens. **c**, Map4 Ips from S fraction were incubated in phosphatase reaction buffer for 15 min at 37° C in – or + active PP1α and then probed for indicated antigens.

To reinforce the finding of MAP-PP1 binding depended on i-Cdk1, we analyzed Map4 and ch-Tog interaction with PP1α under Wee1 downregulation conditions. Prometaphase-arrested control-siRNA- and Wee1-siRNA-treated cells were released into M/C medium for 80 minutes and Map4 and ch-Tog Ips were performed from total extracts (in 250 mM NaCl). PP1α was found to interact with these MAPs in control cells but not in Wee1-siRNA-treated cells (Figure 24a, b, lane 7 and 8, respectively) nor in control cells maintained in the presence of nocodazole (Figure 24a, b, lane 6). PP1α-Map4 and PP1α-ch-Tog binding were restored by low-RO addition (Figure 24a, b, lane 9). Thus, the MT-associated i-Cdk1 allowed active PP1α to interact with Map4 and ch-Tog, promoting their dephosphorylation.

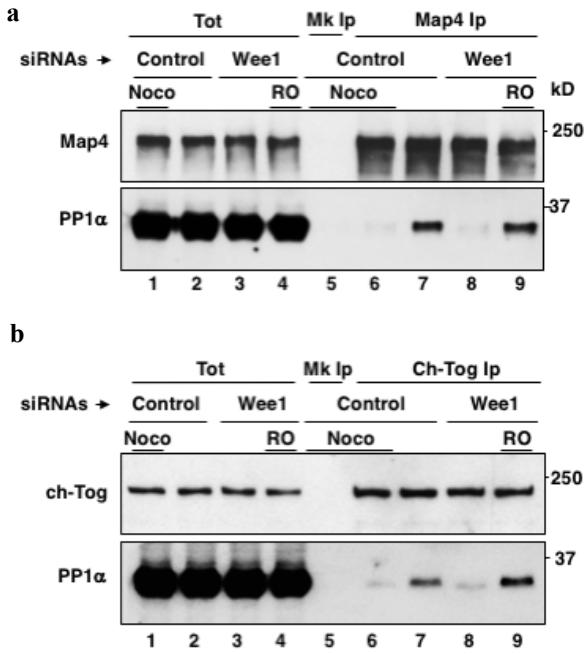

Figure 24 | Spindle-localized MAP interaction with PP1 relies on i-Cdk1. a, **b**, Non-targeting-siRNA- (Control) and Wee1-siRNA-treated (Wee1) hTERT-RPE1 cells were arrested at prometaphase by nocodazole treatment and released into M/C medium for 80 min incubation. A sample of Control cells received nocodazole at time 0 (Noco) and a sample of Wee1-siRNAs cells received low-RO at 60 min of

incubation (RO). Cells were lysed in high salt buffer and **a**, Map4 or **b**, ch-Tog Ips were probed for indicated antigens (lanes 1-4, total lysates; Mk Ip: mock Ips from Noco cell lysates).

PP1 interact with their substrates through specific domains and one of the most conserved among them is R/KxVxF/W - where x represents any aa – motif (Meiselbach *et al.,* 2006; Hendrickx *et al.,* 2009; Heroes *et al.,* 2013). Map4 318-322 residues contain the putative PP1-binding consensus sequence KDVRW. By mutating KDVRW into KDARA in tGFP-Map4-WT expression vector, we produced a Map4 mutant version impaired in PP1 binding (tGFP-Map4-PP1-KO). Indeed, when tGFP-Map4-WT and tGFP-Map4-PP1-KO were expressed at comparable levels and isolated from Meta cells, tGFP-Map4-WT but not with tGFP-Map4-PP1-KO associated with PP1α (Figure 25a). In addition, we analyzed the distribution between S and P fractions of tGFP-Map4-WT and tGFP-Map4-PP1-KO proteins in Meta cells, and found that tGFP-Map4-WT was readly detectable in P fraction while tGFP-Map4-PP1-KO substantially remained in S fraction (Figure 25b). These findings indicate that PP1-dependent Map4 dephosphorylation is crucial for spindle localization of the MAP. We conclude that i-Cdk1 is required for reversal of stabilizing MAPs inhibitory phosphorylation by PP1 in order to promote spindle MT growth and stability.

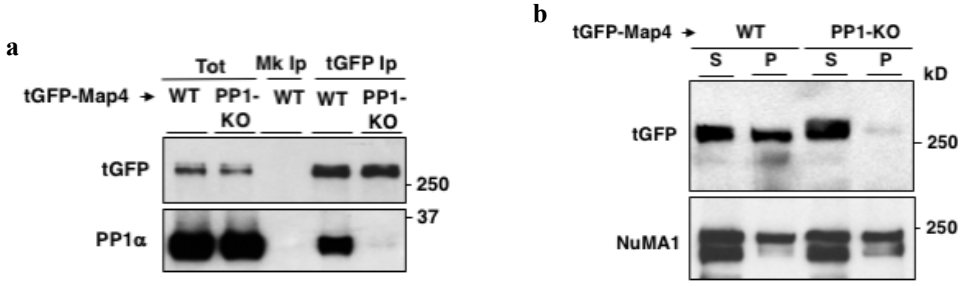

Figure 25 | PP1-dependent dephosphorylation is required for Map4 localization at spindle structures. a, **b**, hTERT-RPE1 cells were transfected with tGFP-Map4 wild type (WT) and mutant tGFP-Map4-impaired in PP1 binding (PP1-KO) expression plasmids and arrested at metaphase. **a**, Cells were lysed in high salt buffer, processed for tGFP Ips and probed for indicated antigens. **b**, S and P fractions were isolated and probed for indicated antigens.

VI.5 Spindle-bound γ-tubulin and nucleating MTs bind and foster i-Cdk1

To dissect the molecular bases of i-Cdk1 interaction with spindle structures, we first probed cyclin B1 Ips from S and P fractions of Meta cells shown in Figure 18c for γ-tubulin and found that γ-tubulin physical interacted with cdk1 selectively in P fraction (Figure 26a). When γ-tubulin Ips from S and P fractions of Pro cells were probed for cdk1 and Wee1, we found that in the P fraction γ-tubulin selectively interacted with Wee1 and i-Cdk1 (Figure 26b). These findings let us to conclude that centrosomes aggregate with Wee1 to promote i-Cdk1.

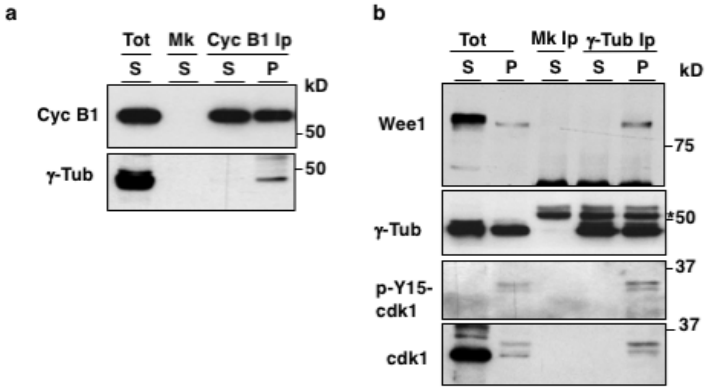

Figure 26 | γ-tubulin aggregates with Wee1 and fosters i-Cdk1. a, Cyclin B1 Ips described in Figure 18c were probed for γ-tubulin. **b**, S and P fractions of Pro hTERT-RPE1 cells were processed for γ-tubulin Ips and probed for indicated antigens.

We have previously shown that i-Cdk1 and Wee1 in P fraction of Meta cells were increased compared to their amounts in P fraction of Pro cells, suggesting a mutual relation between MT polymerization and i-Cdk1 enrichment (see Figure 18a, b). In addition, Map4 and ch-Tog binding to i-Cdk1 was exclusively found in P fraction of Meta cells (see Figure 22a, b). To better estimate the repartition of the Cdk1 inhibitory pathway players between S and P fractions in Pro and Meta cells, the P fractions were enriched 10 folds over the S fractions before proceeding to SDS/PAGE. Meta cells P fraction showed higher Wee1 amounts relatively to Pro cells P fraction and Myt1 also complied

with this trend even if to a much lesser extent (Figure 27a). Thus, Wee1 and Myt1 enrichment in Meta cell P fraction paralleled spindle MT polymerization. Instead, no changes in distribution between P fractions in Meta and Pro cells were detected for Cdc25 phosphatase family members (Cdc25A, Cdc25B, Cdc25C; Figure 27a). Thus, these findings suggest that Wee1, and some Myt1, aggregated with spindle MTs while no Cdc25 members were enriched at these structures (Figure 27a). Mitotic spindle localization of Wee1 was also confirmed by IF (Figure 27b). These data indicate that during mitosis centrosomes, and perhaps intra-spindle γ-tubulin nucleating centers, along with their radiating MTs serve to promote Cdk1 inhibitory phosphorylation, insulating a Cdk1 fraction from the cytoplasmic auto-activatory loops. This seems achieved through Wee1 aggregation with polymerizing MTs and Cdc25 exclusion from them, thereby locally off balancing the Cdk1 auto-activatory loops that instead sustain Cdk1 activity in the cytoplasm. To corroborate this hypothesis, concentrated cytoplasmic extracts from Pro HeLa cells were incubated with nocodazole or with the MT stabilizer paclitaxel at 23° C for 20 minutes to destabilize or stabilize MTs, respectively. Insoluble pellets were isolated, eluted and analyzed (Visconti *et al.,* 2012). Indeed, the pellets of extracts treated with paclitaxel aggregated with Wee1 and i-Cdk1 but not with Cdc25 family members (Figure 27c).

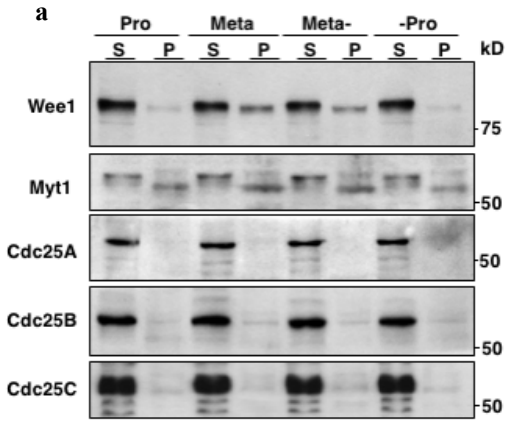

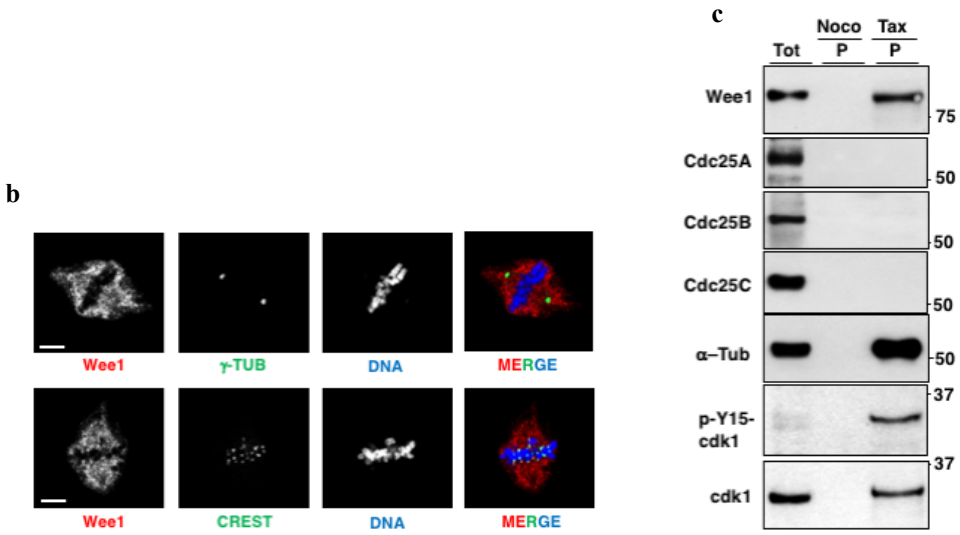

Figure 27 | Polymerizing spindle MTs bind to i-Cdk1 and promote its formation. **a**, S and P fractions from Pro, Meta, Meta- and -Pro hTERT-RPE cells as described in Figure 18, b. P fraction was enriched 10 folds over S fraction; samples were probed for indicated antigens. **b**, Growing hTERT-RPE1 cells were treated with MG-132 for 20 min, fixed and stained for indicated antigens. Scale bar: 5µm. **c**, Eluates from pellet of mitotic HeLa cell extracts (P) were incubated with nocodazole (Noco) or paclitaxel (Tax) and then probed for indicated antigens; Tot: 1/20 of total extract.

Thus, we conclude that during mitosis two spatially separated and functionally opposing Cdk1 fractions coexist. The bulk of Cdk1 in mitosis is active and sustained by auto-activatory loops to antagonize MT polymerization in the cytoplasm by phosphorylating stabilizing MAPs. At the same time, centrosomes, and perhaps intra-spindle γ-tubulin nucleating centers, together with their nucleating MTs promote compartmentalized inhibition of Cdk1 to locally allow PP1 to reverse inhibitory MAP phosphorylation and promote spindle MT growth (Mchedlishvili *et al.,* 2018; Woodruff *et al.,* 2017).

VII. DISCUSSION

VII. DISCUSSION

VII. 1 Cdk1 activity is partially restrained during mitosis

T14 and Y15 have been identified as the major Cdk1 regulatory sites in vertebrate at the G2/M transition of the cell cycle (Krek *et al.,* 1991a). Both residues are maximally phosphorylated during G2 phase by Myt1 and Wee1 kinases to ensure Cdk1 inactivity and allow interphase stages completion (Hunt, 2013). Reversal of Cdk1 inhibitory phosphorylation at T14 and Y15 by Cdc25 phosphatase represents the limiting step for controlling entry into mitosis (Krek *et al.,* 1991a). Once activated, Cdk1 itself maintains its activity priming positive feedback loops that maintain T14 and Y15 residues dephosphorylated throughout mitosis until the metaphase to anaphase transition, when Cdk1 activity drops as a consequence of cyclin B degradation (Hunt, 2013; see Figure 7).

Cdk1 activation drives dramatic cytoskeleton reorganization at mitosis onset as a result of its disassembly-promoting activity on cytoplasmic MTs (Lieuvin *et al.,* 1994) (see Figure 11). The MT polymerization counteracting activity of Cdk1 has been extensively showed in literature, indeed the microinjection of active Cdk1 both into starfish oocytes and xenopus egg extracts and rat fibroblasts has been shown to induce complete destabilization of interphase MTs (Lamb *et al.,* 1990; Verde *et al.,* 1990; Verde *et al.,* 1992; see Figure 11).

In accordance with these findings, the premature activation of Cdk1 resulting from the simultaneous mutation of T14 and Y15 into non-phosphorylatable residues (cdk1AF) causes premature interphase MT destabilization and entry into mitosis (Krek *et al.,* 1991b; see Figure 8). However, cells expressing cdk1AF failed to assemble mitotic spindles (see Figure 8). These mitotic defects were interpreted as a result of mitosis onset in the presence of incomplete DNA replication (Krek *et al.,* 1991b).

We asked whether lack of Cdk1 inhibitory phosphorylation would directly affect spindle assembly. To avoid early Cdk1 activation and ensure DNA replication completion, we transfected cells with either cdk1AF mutant or Wee1-siRNAs and we inhibited Cdk1 activity by high-RO treatment 6 hours post transfection for further 16 hours incubation, to allow DNA replication completion and to synchronize them at G2/M transition (see Figure 15 and 14b, respectively). We found that the defects in spindle assembly occurred also post G2 release, making us to exclude they were attributable to Cdk1 detrimental activity during S phase, but rather they were a consequence of Cdk1 hyperactivity during M phase. Indeed, slight Cdk1 inhibition via low-RO adding to both cells expressing Cdk1AF and Wee1-siRNA-treated cells restored correct bipolar spindle assembly (see Figure 15 and 14b, respectively). This data demonstrated that partial Cdk1 activity inhibition during mitosis is a requirement for mitotic spindle assembly. This led us to hypothesize that Cdk1 is not, as believed, fully active in mitosis but some fraction of it is in inhibited form (i-Cdk1). Evidence that i-Cdk1 is present in Xenopus and mouse meiotic and mitotic extract eggs had already been reported (D'Angiolella *et al.,* 2007; Oh *et al.,* 2011; see Figure 9). Here we unveiled the existence of an unexpected form of Cdk1 (i-Cdk1) that is inhibited by phosphorylation in mitosis and its crucial role for the assembly of the mitotic spindle.

VII. 2 I-Cdk1 is selectively bound to spindle structures

To dissect the localization of i-Cdk1 during mitosis, we adapted a method for cell fractionation, obtaining a fraction made of soluble cytoplasmic components (S fraction) and an insoluble fraction consisting of spindle structures and tightly bound proteins (P fraction) (Silljé *et al.,* 2006; see Materials and Methods section). Through this approach we found that i-Cdk1 was exclusively bound to spindle structures (P fractions; see Figure 18a, b).

In addition, we found i-Cdk1 directly interacted with γ-tubulin localized at spindle structures but not with free cytoplasmic γ-tubulin (see Figure 26b). Based on the most recent data concerning the MT structure, γ-tubulin acts as nucleating factor for MTs not only at centrosomes associating with GCP proteins to form γ-TuRCs, but also localizing along a pre-existing MT lattice to promote branching MT fiber nucleation through effector proteins aid (David *et al.,* 2019; Thawani *et al.,* 2019; Alfaro-Aco *et al.,* 2020). Thus, as shown by IF, i-Cdk1 seems to localize at MT nucleation centers, spanning from centrosomes up to extend the entire spindle (see Figure 17).
Moreover, we found i-Cdk1 directly interacted with the MT associated pools of Map4 and ch-Tog (see Figure 22a, b).

VII. 3 I-Cdk1 allows PP1 to locally activate during spindle assembly

PP1 are crucial Cdk1-counteracting phosphatases (Qian *et al.,* 2013). Their activity is directly regulated by Cdk1 phosphorylation of inhibitory sites at their catalytic subunits, such as T320 residue of PP1α isoform (Dohadwala *et al.,* 1994; Kwon *et al.,* 1997). Thus, PP1 activity is suppressed by Cdk1 until metaphase to anaphase transition. Interestingly, we found that the spindle-bound portion of PP1α was dephosphorylated at T320, suggesting its local activation during mitosis (see Figure 23a).
Map4 and ch-Tog pools localized at mitotic structure (P fractions) seemed to be in a hypophosphorylated state compared to their cytosolic forms (S fractions; see Figure 18a, b). In particular, we found that S787 residue on Map4, which had been identified as an M-phase specific and Cdk1 phosphorylation-dependent site (Ookata *et al.,* 1997; Kitazawa et al., 2000), was dephosphorylated when Map4 associated with spindle structures (P fractions; see Figure 21b). Moreover, Map4 dephosphorylation at S787 is PP1α-mediated (see Figure 23c). We also demonstrated that spindle-bound

Map4 and ch-Tog directly interacted with active PP1α (see Figure 22a, b, respectively). Moreover, PP1 binding to these MAPs relied on i-Cdk1, since lack of Cdk1 inhibitory phosphorylation impeded PP1-Map4 and PP1-ch-Tog interaction (see Figure 24a, b, respectively). In turn, PP1 binding to Map4 regulated its localization at spindle structures, since abolishing of Map4-PP1-binding site (tGFP-Map4-PP1-KO mutant) prevented its distribution at P fraction (see Figure 25b).

We found that i-Cdk1 increased during spindle MT polymerization and spindle assembly (see Figure 18a, b) and that polymerizing spindle MTs recruited Wee1 but not Cdc25, thus controlling Cdk1 activity in a compartmentalized fashion, insulated from the cytoplasmic auto-activatory loops (see Figure 27a). We concluded that this compartmentalized control of Cdk1 is required to locally reverse inhibitory phosphorylation of spindle MAPs. Thus, spindle-bound i-Cdk1 allows PP1 to locally dephosphorylate MAPs to reactivate their MT stabilization properties and promote spindle assembly.

Our findings provide an explanation for how cells in mitosis destabilize cytoplasmic MTs and, at the same time, allow growth of spindle MTs and spindle assembly.

VIII. CONCLUSIONS

VIII. CONCLUSIONS

Cdk1 is largely active during mitosis and its activity is sustained by positive feedback loops within the cytoplasm where it induces MTs to destabilize and dissolve via MAP phosphorylation (Pomerening *et al.,* 2003; Hunt, 2013; Novák *et al.,* 2021). However, we find that a small fraction of Cdk1 escapes the activatory loops in mitosis and undergoes inactivation by phosphorylation (i-Cdk1). I-Cdk1 exhibits a defined localization at spindle structures. Thus, at the onset of mitosis, the MT polymerization-counteracting activity of active Cdk1 clears pre-existing interphase MTs and blocks further MT polymerization in the cytoplasm to enable safe chromosome movements. At the same time, at centrosomes, and perhaps at intra-spindle γ-tubulin nucleating centers and along their nucleating MTs, a fraction of Cdk1 is inhibited by phosphorylation via reversal of cytoplasmic feedback loops trend (David *et al.,* 2019; Thawani *et al.,* 2020; Woodruff *et al.,* 2017). Localized Cdk1 inhibition is required to reverse inhibitory MAP phosphorylation to locally restore their ability to stabilize MTs (Mchedlishvili *et al.,* 2018). In particular, i-Cdk1 allows active PP1 to interact with MAPs and reverse their inhibitory phosphorylation to promote spindle MT growth and stabilization.

In conclusion, our data demonstrate that correct spindle assembly at mitosis requires partial and localized Cdk1 activity restraint. This finding provides a possible explanation for the paradoxical coexistence of Cdk1 destabilizing activity on MTs and simultaneous spindle MT elongation and spindle assembly (Figure 28).

Localized control of Cdk1 activity might also be supported by other mechanisms, in addition to inhibitory phosphorylation, and help to promote anaphase onset upon spindle assembly (Yim *et al.,* 2010; Schmidt *et al.,* 2021).

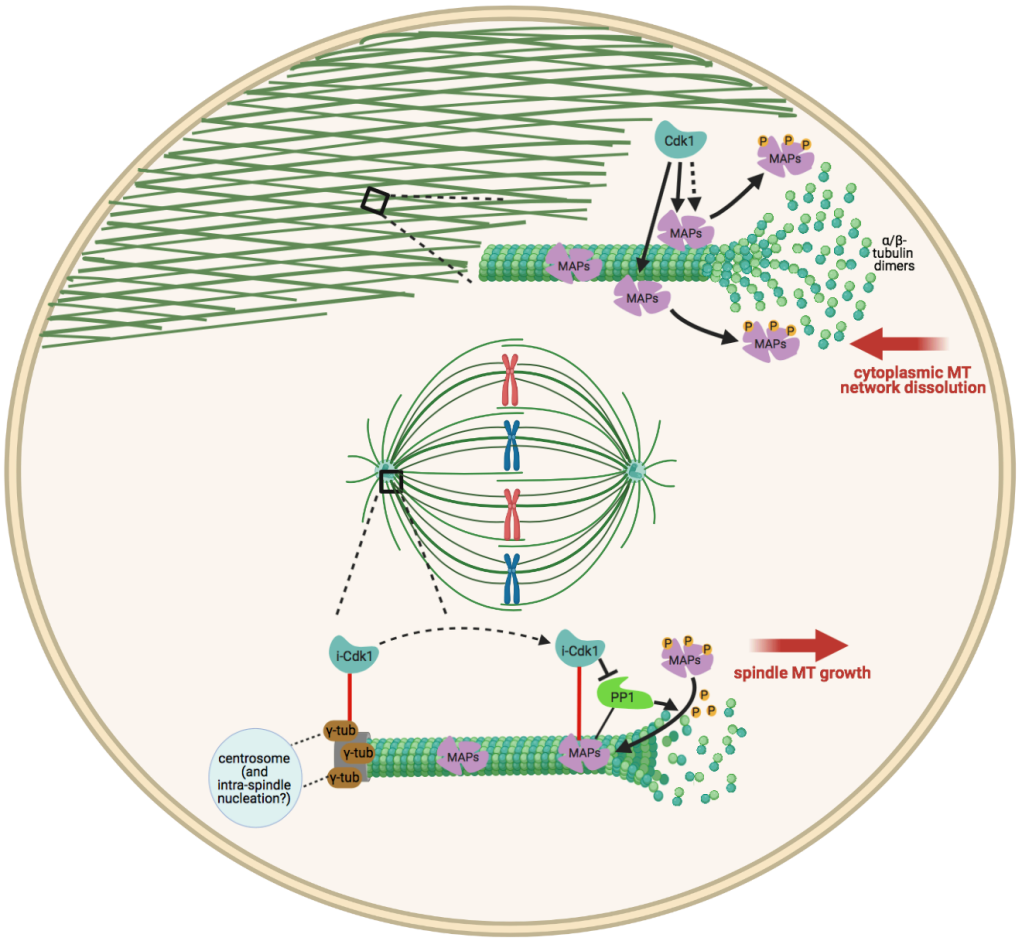

Figure 28 | Localized Cdk1 activity control for mitotic spindle assembly. In mitosis, positive feedback loops maintain high Cdk1 activity in the cytoplasm. Active Cdk1 destabilizes cytoplasmic MTs by directly (continuous arrow) or indirectly (dashed arrow) phosphorylating and inhibiting stabilizing MAPs. At the same time, at centrosomes and along their nucleating MTs, a fraction of Cdk1 escapes the cytoplasmic feedback loops and is inhibited by phosphorylation (i-Cdk1). Localized i-Cdk1 allows PP1 to reverse inhibitory phosphorylation of MAPs and promote spindle MT growth.

IX. ACKNOWLEDGEMENTS

IX. ACKNOWLEDGEMENTS

I would like to express my gratitude to Professor Domenico Grieco, who imparted practical and theoretical knowledge about the basic mechanisms of cell division to me. I am grateful to him for the skillful guidance, constant support and stoic patience over these years and for allowing me the opportunity to work in the research environment that stimulates original thinking and initiative, which he created. I will always be indebted to him for sparking and cultivating my interest in molecular medicine.

I would like to acknowledge my research labmates Francesco Febbraro and Caterina Pisauro. Thank you for the practical help, encouragement, cups of coffee and infectious smile.

I am thankful to Doctor Roberta Visconti for teaching me basic molecular biology techniques.

I would also like to acknowledge Professors Vittorio Enrico Avvedimento, Massimo Santoro, Lucio Nitsch for helping me during the PhD course and for their helpful suggestions and the external members of the PhD committee for their thoughtful comments.

I am as well grateful to Associazione Italiana per la Ricerca sul Cancro (AIRC) for supporting Professor D. Grieco work.

X. LIST OF PUBLICATIONS

X. LIST OF PUBLICATIONS

1. **Serpico AF**, Febbraro F, Pisauro C, Grieco D. Compartmentalised control of Cdk1 drives mitotic spindle assembly. bioRxiv. 2021;04.20.440650.

2. **Serpico AF**, Visconti R, Grieco D. Exploiting immune-dependent effects of microtubule-targeting agents to improve efficacy and tolerability of cancer treatment. Cell Death Dis. 2020;11(5):361.

3. **Serpico AF**, Grieco D. Recent advances in understanding the role of Cdk1 in the Spindle Assembly Checkpoint. F1000Res. 2020;9:F1000 Faculty Rev-57.

4. **Serpico AF**, D'Alterio G, Vetrei C, Della Monica R, Nardella L, Visconti R, Grieco D. Wee1 Rather Than Plk1 Is Inhibited by AZD1775 at Therapeutically Relevant Concentrations. Cancers (Basel). 2019;11(6):819.

5. Cervone N, Della Monica R, **Serpico AF**, Vetrei C, Scaraglio M, Visconti R, Grieco D. Evidence that PP2A activity is dispensable for spindle assembly checkpoint-dependent control of Cdk1. Oncotarget. 2017;9(7):7312-7321.

6. Della Monica R, Visconti R, Cervone N, **Serpico AF,** Grieco D. Fcp1 phosphatase controls Greatwall kinase to promote PP2A-B55 activation and mitotic progression. Elife. 2015;4:e10399

XI. REFERENCES

XI. REFERENCES

1. Aizawa H, Kamijo M, Ohba Y, Mori A, Okuhara K, Kawasaki H, Murofushi H, Suzuki K, Yasuda H. Microtubule destabilization by cdc2/H1 histone kinase: phosphorylation of a "pro-rich region" in the microtubule-binding domain of MAP-4. Biochem Biophys Res Commun. 1991;179(3):1620-1626.

2. Akhmanova A, Steinmetz MO. Microtubule minus-end regulation at a glance. J Cell Sci. 2019;132(11):jcs227850.

3. Alfaro-Aco R, Thawani A, Petry S. Biochemical reconstitution of branching microtubule nucleation. Elife. 2020;9:e49797.

4. Belmont LD, Hyman AA, Sawin KE, Mitchison TJ. Real-time visualization of cell cycle-dependent changes in microtubule dynamics in cytoplasmic extracts. Cell. 1990;62(3):579-589.

5. Burbank KS, Mitchison TJ. Microtubule dynamic instability. Curr Biol. 2006;16(14):R516-517.

6. Castro A, Bernis C, Vigneron S, Labbé JC, Lorca T. The anaphase-promoting complex: a key factor in the regulation of cell cycle. Oncogene. 2005;24:314-325.

7. Chang W, Gruber D, Chari S, Kitazawa H, Hamazumi Y, Hisanaga SI, Bulinski JC. Phosphorylation of MAP4 affects microtubule properties and cell cycle progression. J Cell Sci. 2001;114(15):2879-2887.

8. Charrasse S, Schroeder M, Gauthier-Rouviere C, Ango F, Cassimeris L, Gard DL, Larroque C. The TOGp protein is a new human microtubule-associated protein homologous to the Xenopus XMAP215**.** J Cell Sci. 1998;111(10):1371-1383.

9. Charrasse S, Lorca T, Dorée M, Larroque C. The *Xenopus* XMAP215 and its human homologue TOG proteins interact with cyclin B1 to target p34cdc2 to microtubules during mitosis. Exp Cell Res. 2000;254(2):249–256.

10. Clute P, Pines J. Temporal and spatial control of cyclin B1 destruction in metaphase. Nat Cell Biol. 1999;1(2):82-87.

11. D'Angiolella V, Palazzo L, Santarpia C, Costanzo V, Grieco D. Role for non- proteolytic control of M-phase-promoting factor activity at M-phase exit. PLoS One. 2007;2(2):e247.

12. David AF, Roudot P, Legant WR, Betzig E, Danuser G, Gerlich DW. Augmin accumulation on long-lived microtubules drives amplification and kinetochore-directed growth. J Cell Biol. 2019;218(7):2150-2168.

13. DeLuca, JG, Musacchio A. Structural organization of the kinetochore-microtubule interface. Curr Opin Cell Biol. 2012;24(1):48–56.

14. Dohadwala M, da Cruz e Silva EF, Hall FL, Williams RT, Carbonaro-Hall DA, Nairn AC, Greengard P, Berndt N. Phosphorylation and inactivation of protein phosphatase 1 by cyclin-dependent kinases. Proc Natl Acad Sci USA. 1994;91(14):6408–6412.

15. Doxsey S. Re-evaluating centrosome function. Nat Rev Mol Cell Biol. 2001;2(9):688-698.

16. Drewes G, Ebneth A, Mandelkow EM. MAPs, MARKs and microtubule dynamics. Trends Biochem Sci. 1998;23(8):307–311.

17. Fattaey A, Booher RN. Myt1: a Wee1-type kinase that phosphorylates Cdc2 on residue Thr14. Prog Cell Cycle Res. 1997;3:233-240.

18. Fry AM, Sampson J, Shak C, Shackleton S. Recent advances in pericentriolar material organization: ordered layers and scaffolding gels. F1000Res. 2017;6:1622.

19. Gard DL, Kirschner MW. A microtubule-associated protein from Xenopus eggs that specifically promotes assembly at the plus-end. J Cell Biol. 1987; 105(5):2203-2215.

20. Gautier J, Norbury C, Lohka M, Nurse P, Maller J. Purified maturation-promoting factor contains the product of a Xenopus homolog of the fission yeast cell cycle control gene *cdc2*$^{+}$. Cell. 1988;54(3):433-439.

21. Gavet O, Pines J. Progressive activation of CyclinB1-Cdk1 coordinates entry to mitosis. Dev Cell. 2010;18(4):533-543.

22. Gergely F, Draviam VM, Raff JW. The ch-TOG/XMAP215 protein is essential for spindle pole organization in human somatic cells. Genes Dev. 2003;17(3):336-341.

23. Goodson HV, Jonasson EM. Microtubules and microtubule-associated proteins. Cold Spring Harb Perspect Biol. 2018;10(6):a022608.

24. Goshima G, Mayer M, Zhang N, Stuurman N, Vale RD. Augmin: a protein complex required for centrosome-independent microtubule generation within the spindle. J Cell Biol. 2008;181(3):421–429.

25. Gruss OJ, Wittmann M, Yokoyama H, Pepperkok R, Kufer T, Sillje H, Karsenti E, Mattaj IW, Vernos I. Chromosome-induced microtubule assembly mediated by TPX2 is required for spindle formation in HeLa cells. Nat Cell Biol. 2002;4(11):871–879.

26. Gutiérrez-Caballero C, Burgess SG, Bayliss R, Royle SJ. TACC3-ch-TOG track the growing tips of microtubules independently of clathrin and Aurora-A phosphorylation. Biol Open. 2015;4(2):170-179.

27. Hégarat N, Rata S, Hochegger H. Bistability of mitotic entry and exit switches during open mitosis in mammalian cells. Bioessays. 2016;38(7):627-643.

28. Hendrickx A, Beullens M, Ceulemans H, Abt TD, Eynde AV, Nicolaescu E, Lesage B, Bollen M. Docking motif-guided mapping of the interactome of protein phosphatase-1. Chem Biol. 2009;16(4):365-371.

29. Heroes W, Lesage B, Gørnemann J, Beullens M, Meervelt LV, Bollen M. The PP1 binding code: a molecular-lego strategy that governs specificity. FEBS J. 2013;280(2):584-595.

30. Hoffmann I, Clarke PR, Marcote MJ, Karsenti E, Draetta G. Phosphorylation and activation of human cdc25-C by cdc2-cyclin B and its involvement in the self-amplification of MPF at mitosis. EMBO J. 1993;12(1):53-63.

31. Hueschen CL, Kenny SJ, Xu K, Dumont S. NuMA recruits dynein activity to microtubule minus-ends at mitosis. eLife. 2017;6:e29328.

32. Hunt T. On the regulation of protein phosphatase 2A and its role in controlling entry into and exit from mitosis. Adv Biol Regul. 2013;53(2)173-178.

33. Kamasaki T, O'Toole E, Kita S, Osumi M, Usukura J, McIntosh JR, Goshima G. Augmin-dependent microtubule nucleation at microtubule walls in the spindle. J Cell Biol. 2013;202(1):25–33.

34. Kavallaris M, Don S, Verrills NM. Microtubule-Associated Proteins and Microtubule-Interacting Proteins. In: Fojo T, editor. The Role of Microtubules in Cell Biology, Neurobiology, and Oncology. Cancer Drug Discovery and Development. New York: Humana Press; 2008. p. 83-104.

35. Kinoshita K, Habermann B, Hyman AA. XMAP215: a key component of the dynamic microtubule cytoskeleton. Trends Cell Biol. 2002;12(6):267-273.

36. Kirschner M, Mitchison T. Beyond self-assembly: from microtubules to morphogenesis. Cell. 1986a;45(3):329–342.

37. Kirschner MW, Mitchison T. Microtubule dynamics. Nature. 1986b;324:621.

38. Kishimoto T. Entry into mitosis: a solution to the decades-long enigma of MPF. Chromosoma. 2015;124:417–428.

39. Kitazawa H, Iida J, Uchida A, Haino-Fukushima K, Itoh TJ, Hotani H, Ookata K, Murofushi H, Bulinski JC, Kishimoto T, Hisanaga SI. Ser787 in the Proline-Rich Region of Human MAP4 is a Critical Phosphorylation Site that Reduces its Activity to Promote Tubulin Polymerization. Cell Struct Funct. 2000;25(1):33-39.

40. Krek W, Nigg EA. Cell cycle regulation of vertebrate p34cdc2 activity: identification of Thr161 as an essential in vivo phosphorylation site. New Biol. 1992;4(4):323–329.

41. Krek W, Nigg EA. Differential phosphorylation of vertebrate p34cdc2 kinase at the G1/S and G2/M transitions of the cell cycle: identification of major phosphorylation sites. EMBO J. 1991a;10(2):305-316.

42. Krek W, Nigg EA. Mutations of p34cdc2 phosphorylation sites induce premature mitotic events in HeLa cells: evidence for a double block to p34cdc2 kinase activation in vertebrates. EMBO J. 1991b;10(11):3331-3341.

43. Kumagai A, Dunphy WG. Regulation of the cdc25 protein during the cell cycle in Xenopus extracts. Cell. 1992;70(1):139-151.

44. Kwon YG, Lee SY, Choi Y, Greengard P, Nairn AC. Cell cycle-dependent phosphorylation of mammalian protein phosphatase 1 by cdc2 kinase. Proc Natl Acad Sci USA. 1997;94(6):2168–2173.

45. Labbé JC, Capony JP, Caput D, Cavadore JC, Derancourt J, Kaghad M, Lelias JM, Picard A, Dorée M. MPF from starfish oocytes at first meiotic metaphase is a heterodimer containing one molecule of cdc2 and one molecule of cyclinB. EMBO J. 1989; 8(10):3053-3058.

46. Lamb NJ, Fernandez A, Watrin A, Labbé JC, Cavadore JC. Microinjection of p34cdc2 kinase induces marked changes in cell shape, cytoskeletal

organization, and chromatin structure in mammalian fibroblasts. Cell. 1990;60(1):151-165.

47. Lecland N, Lüders J. The dynamics of microtubule minus ends in the human mitotic spindle. Nat Cell Biol. 2014;16(8):770-778.

48. Lee MJ, Gergely F, Jeffers K, Peak-Chew SY, Raff JW. Msps/XMAP215 interacts with the centrosomal protein D-TACC to regulate microtubule behaviour. Nat Cell Biol. 2001;3(7):643-649.

49. Lieuvin A, Labbé JC, Dorée M, Job D. Intrinsic Microtubule Stability in Interphase Cells. J Cell Biol. 1994;124(6):985-996.

50. Liu F, Stanton JJ, Wu Z, Piwnica-Worms H. The human Myt1 kinase preferentially phosphorylates Cdc2 on threonine 14 and localizes to the endoplasmic reticulum and Golgi complex. Mol Cell Biol. 1997;17(2):571-583.

51. Liu P, Zupa E, Neuner A, Böhler A, Loerke J, Flemming D, Ruppert T, Rudack T, Peter C, Spahn C, Gruss OJ, Pfeffer S, Schiebel E. Insights into the assembly and activation of the microtubule nucleator γ-TuRC**.** Nature. 2019;578(2020):467-471.

52. Lohka MJ, Hayest MK, Maller JL. Purification of maturation-promoting factor, an intracellular regulator of early mitotic events. Proc Natl Acad Sci USA. 1988;85:3009:3013.

53. Margolin G, Gregoretti IV, Cickovski TM, Li C, Shi W, Alber MS, Goodson HV. The mechanisms of microtubule catastrophe and rescue: implications from analysis of a dimer-scale computational model. Mol Biol Cell. 2012;23(4):642-656.

54. Masui Y, Markert CL. Cytoplasmic control of nuclear behavior during meiotic maturation of frog oocytes. J Exp Zool. 1971;177(2):129–145.

55. Mchedlishvili N, Matthews HK, Corrigan A, Baum B. Two-step interphase microtubule disassembly aids spindle morphogenesis. BMC Biology. 2018;16:14.

56. McGowan CH, Russel P. Cell cycle regulation of human WEE1. EMBO J. 1995;14(10):2166-2175.

57. McIntosh JR. Mitosis. Cold Spring Harb Perspect Biol. 2016;8:a023218.

58. Meiselbach H, Sticht H, Enz R. Structural analysis of the protein phosphatase 1 docking motif: molecular description of binding specificities identifies interacting proteins. Chem Biol. 2006;13(1):49-59.

59. Meunier S, Vernos I. Acentrosomal Microtubule Assembly in Mitosis: The Where, When, and How. Trends Cell Biol. 2016;26(2):80–87.

60. Morgan D, Desai A, Edgar B, Glotzer M, Heald R, Karsenti E, Nasmyth K, Pines J, Sherr C. The cell cycle. In: Alberts B, Johnson A, Lewis J, Raff M, Roberts K, Walter P, editors. Molecular biology of the cell. 6th ed. New York: Garland Science; 2015. p. 963-1020.

61. Mueller PR, Coleman TR, Kumagai A, Dunphy WG. Myt1: a membrane-associated inhibitory kinase that phosphorylates Cdc2 on both threonine-14 and tyrosine-15. Science. 1995;270(5233):86-90.

62. Musacchio A, Salmon ED. The spindle-assembly checkpoint in space and time. Nat Rev Mol Cell Biol. 2007;8(5):379-393.

63. Nakajima H, Toyoshima-Morimoto F, Taniguchi E, Nishida W. Identification of a consensus motif for Plk (Polo-like kinase) phosphorylation reveals Myt1 as a Plk1 substrate. J Biol Chem. 2004;278:25277–25280.

64. Nguyen HL, Chari S, Gruber D, Lue CM, Chapin SJ, Bulinski JC. Overexpression of full- or partial-length MAP4 stabilizes microtubules and alters cell growth**.** J Cell Sci. 1997;110(2):281-294.

65. Nguyen HL, Gruber D, Bulinski JC. (1999). Microtubule- associated protein 4 (MAP4) regulates assembly, protomer-polymer partitioning and synthesis of tubulin in cultured cells. J. Cell Sci. 1999;112:1813- 1824.

66. Nigg EA. Cellular substrates of p34(cdc2) and its companion cyclin-dependent kinases. Trends Cell Biol. 1993;3(9):296-301.

67. Novak B, Tyson JJ. Modeling the Cell Division Cycle: M-phase Trigger, Oscillations, and Size Control. J Theor Biol. 1993;165:101–134.

68. Novák B, Tyson JJ, Mechanisms of signalling-memory governing progression through the eukaryotic cell cycle. Curr Opin Cell Biol. 2021;69:7-16.

69. O'Farrell PH. Triggering the all-or-nothing switch into mitosis. Trends Cell Biol. 2001;11(12):512–519.

70. Oh JS, Susor A, Conti M. Protein tyrosine kinase Wee1B is essential for metaphase II exit in mouse oocytes. Science. 2011;332(6028):462-465.

71. Ohkura H, Garcia MA, Toda T. Dis1/TOG universal microtubule adaptors - one MAP for all? J Cell Sci. 2001;114(21):3805-3812.

72. Ookata K, Hisanaga S, Bulinski JC, Murofushi H, Aizawa H, Itoh TJ, Hotani H, Okumura E, Tachibana K, Kishimoto T. Cyclin B interaction with microtubule-associated protein 4 (MAP4) targets p34cdc2 kinase to microtubules and is a potential regulator of M-phase microtubule dynamics. J Cell Biol. 1995;128(5):849–862.

73. Ookata K, Hisanaga S, Sugita M, Okuyama A, Murofushi H, Kitazawa H, Chari S, Bulinski JC, Kishimoto T. MAP4 is the in vivo substrate for CDC2 kinase in HeLa cells: identification of an M-phase specific and a cell cycle-independent phosphorylation site in MAP4. Biochemistry. 1997; 36(50):15873–15883.

74. Parker LL, Piwnica-Worms H. Inactivation of the p34cdc2-cyclin B complex by the human WEE1 tyrosine kinase. Science. 1992;257(5078):1955-1957.

75. Perry JA, Kornbluth S. Cdc25 and Wee1: analogous opposites? Cell Div. 2007;2:12.

76. Petry S. Mechanisms of Mitotic Spindle Assembly**.** Annu Rev Biochem. 2016;85:659–683.

77. Petry S, Pugieux C, Nédélec FJ, Vale RD. Augmin promotes meiotic spindle formation and bipolarity in Xenopus egg extracts. Proc Natl Acad Sci USA. 2011;108(35):14473–14478.

78. Petry S, Vale RD. Microtubule nucleation at the centrosome and beyond. Nat Cell Biol. 2015;17(9):1089-1093.

79. Pomerening JR, Sontag ED, Ferrell JEJ. Building a cell cycle oscillator: hysteresis and bistability in the activation of Cdc2. Nat Cell Biol. 2003;5(4):346-351.

80. Qian J, Winkler C, Bollen M. 4D-networking by mitotic phosphatases. Curr Opin Cell Biol. 2013;25(6):697-703.

81. Remy M, Merdes A, Gregory-Pauron L. Assembly of Gamma-Tubulin Ring Complexes: Implications for Cell Biology and Disease. Prog Mol Biol Transl Sci. 2013;117:511-530.

82. Sampath SC, Ohi R, Leismann O, Salic A, Pozniakovski A, Funabiki H. The chromosomal passenger complex is required for chromatin-induced microtubule stabilization and spindle assembly. Cell. 2004;118(2):187–202.

83. Schmidt AK, Pudelko K, Boekenkamp JE, Berger K, Kschischo M, Bastians H. The p53/p73 - $p21^{CIP1}$ tumor suppressor axis guards against chromosomal instability by restraining CDK1 in human cancer cells. Oncogene. 2021;40(2)436-451.

84. Scrofani J, Sardon T, Meunier S, Vernos I. Microtubule nucleation in mitosis by a RanGTP-dependent protein complex. Curr Biol. 2015;25(2):131–140.

85. Serpico AF, D'Alterio G, Vetrei C, Della Monica R, Nardella L, Visconti R, Grieco D. Wee1 Rather Than Plk1 Is Inhibited by AZD1775 at Therapeutically Relevant Concentrations. Cancers (Basel). 2019;11(6):819.

86. Silljé HHW, Nigg EA. Purification of mitotic spindles from cultured human cells. Methods. 2006;38(1):25-28.

87. Solomon MJ, Lee T, Kirschner MW. Role of phosphorylation in p34cdc2 activation: identification of an activating kinase. Mol Biol Cell. 1992;3(1):13–27.

88. Strausfeld U, Labbè JC, Fesquet D, Cavadore JC, Picard A, Sadhut K, Russell P**,** Dorèe M. Dephosphorylation and activation of a p34*cdc2 1*cyclin B complex *in vitro* by human CDC25 protein. Nature. 1991;351(6323):242-245.

89. Thawani A, Rale MJ, Coudray N, Bhabha G, Stone HA, Shaevitz JW, Petry S. The transition state and regulation of γ-TuRC-mediated microtubule nucleation revealed by single molecule microscopy. Elife. 2020;9:e54253.

90. Thawani A, Stone HA, Shaevitz JW, Petry S. Spatiotemporal organization of branched microtubule networks. Elife.2019;8:e43890.

91. Thron CD. A model for a bistable biochemical trigger of mitosis. 1996;57(2-3):239-251.

92. Tombes RM, Peloquin JG, Borisy GG. Specific association of an M-phase kinase with isolated mitotic spindles and identification of two of its substrates as MAP4 and MAP1B. Cell Regul. 1991;2:861-874.

93. Tovey CA, Conduit PT. Microtubule nucleation by γ-tubulin complexes and beyond. Essays Biochem. 2018;62(6):765-780.

94. Trunnell NB, Poon AC, Kim SY, Ferrell JJE. Ultrasensitivity in the regulation of Cdc25C by Cdk1. Mol Cell. 2011;41(3):263–274.

95. Ubersax JA, Woodbury EL, Quang PN, Paraz M, Justin D. Blethrow JD, Shah K, Shokat KM, Morgan DO. Targets of the cyclin-dependent kinase Cdk1. Nature. 2003;425(6960):859-64.

96. Vasquez RJ, Gard DL, Cassimeris L. Phosphorylation by CDK1 regulates XMAP215 function in vitro. Cell Motil Cytoskelet. 1999;43(4):310–321.

97. Vassilev LT, Tovar C, Chen S, Knezevic D, Zhao X, Sun H, Heimbrook DC, Chen L. Selective small-molecule inhibitor reveals critical mitotic functions of human CDK1. Proc Natl Acad Sci USA. 2006;103(28):10660.

98. Verde F, Dogterom M, Stelzer E, Karsenti E, Leibler S. Control of microtubule dynamics and length by cyclin A- and cyclin B-dependent kinases in *Xenopus* egg extracts. J Cell Biol. 1992;118(5):1097–1108.

99. Verde F, Labbé JC, Dorée M, Karsenti E. Regulation of microtubule dynamics by cdc2 protein kinase in cell-free extracts of *Xenopus* eggs. Nature. 1990;343:233–238.

100. Vertii A, Hehnly H, Doxsey S. The Centrosome, a Multitalented Renaissance Organelle. Cold Spring Harb Perspect Biol. 2016;8:a025049.

101. Visconti R, Della Monica R, Palazzo L, D'Alessio F, Raia M, Improta S, Villa MR, Del Vecchio L, Grieco D. The Fcp1-Wee1-Cdk1 axis affects spindle assembly checkpoint robustness and sensitivity to antimicrotubule cancer drugs. Cell Death Differ. 2015;**22**(9):1551-1560.

102. Visconti R, Palazzo L, Della Monica R, Grieco D. Fcp1-dependent dephosphorylation is required for M-phase-promoting factor inactivation at mitosis exit. Nat Commun. 2012;3:894.

103. Wang G, Jiang Q, Zhang C. The role of mitotic kinases in coupling the centrosome cycle with the assembly of the mitotic spindle. Journal of Cell Science. 2014;127:4111–4122.

104. Wasserman WJ, Masui Y. A cytoplasmic factor promoting oocyte maturation: its extraction and preliminary characterization. Science. 1976;191(4233):1266–1268.

105. Watanabe N, Arai H, Iwasaki J, Shiina M, Ogata K, Hunter T, Osada H. Cyclin-dependent kinase (CDK) phosphorylation destabilizes somatic Wee1 via multiple pathways. Proc Natl Acad Sci USA. 2005;102(33):11663-11668.

106. Watanabe N, Arai H, Nishihara Y, Taniguchi M, Watanabe N, Hunter T, Osada H. M-phase kinases induce phospho-dependent ubiquitination of somatic Wee1 by $SCF^{\beta\text{-}TrCP}$. Proc Natl Acad Sci USA. 2004;101(13):4419-24.

107. Wells WA. Microtubules get a name. J Cell Biol. 2005;168(6):852–853.

108. West RR, Tenbarge KM, Olmsted JB. A Model for Microtubule-associated Protein 4 Structure. J Biol Chem. 1991;266(32):21886-21896.

109. Wollman R, Cytrynbaum EN, Jones JT, Meyer T, Scholey JM, Mogilner A. Efficient chromosome capture requires a bias in the 'search-and-capture' process during mitotic-spindle assembly. Curr Biol. 2005;15(9):828–832.

110. Woodruff JB, Gomes BF, Widlund PO, Mahamid J, Honigmann A, Hyman AA. The centrosome is a selective condensate that nucleates microtubules by concentrating tubulin. Cell. 2017;169(6):1066-1077.

111. Wu J, Akhmanova A. Microtubule-Organizing Centers. Annu Rev Cell Dev Biol. 2017;33:51–75.

112. Wu JQ, Guo JY, Tang W, Yang CS, Freel CD, Chen C, Nairn AC, Kornbluth S. PP1-mediated dephosphorylation of phosphoproteins at mitotic exit is controlled by inhibitor-1 and PP1 phosphorylation. Nat Cell Biol. 2009;11(5):644–651.

113. Wurzenberger C, Gerlich DW. Phosphatases: providing safe passage through mitotic exit. Nat Rev Mol Cell Biol. 2011;12(8):469-482.

114. Yim H, Erikson RL. Cell division cycle 6, a mitotic substrate of polo-like kinase 1, regulates chromosomal segregation mediated by cyclin-dependent kinase 1 and separase. Proc Natl Acad Sci USA. 20120;107(46)19742-19747.

115. Zeng C. NuMA: A Nuclear Protein Involved in Mitotic Centrosome Function. Microsc Res Tech. 2000;49(5):467-477.

116. Zheng Y, Wong ML, Alberts B, Mitchison T. Nucleation of microtubule assembly by a γ-tubulin-containing ring complex. Nature. 1995;378(6557):578-583.